


Article

Single Cell ADNP Predictive of Human Muscle Disorders: Mouse Knockdown Results in Muscle Wasting

Oxana Kapitanisky ¹, Gidon Karmon ¹, Shlomo Sragovich ¹, Adva Hadar ^{1,2}, Meishar Shahoha ³, Iman Jaljuli ⁴, Lior Bikovski ⁵, Eliezer Giladi ¹, Robert Palovics ^{6,7}, Tal Iram ^{6,7} and Illana Gozes ^{1,*} 

¹ The Elton Laboratory for Molecular Neuroendocrinology, Department of Human Molecular Genetics and Biochemistry, Sackler Faculty of Medicine, Sagol School of Neuroscience and Adams Super Center for Brain Studies, Tel Aviv University, Tel Aviv 6997801, Israel; oxana188@hotmail.com (O.K.); gidikarmon@gmail.com (G.K.); srshlomo@gmail.com (S.S.); advaad@gmail.com (A.H.); elieze@tauex.tau.ac.il (E.G.)

² Department of Molecular Genetics, Weizmann Institute of Science, Rehovot 7610001, Israel

³ Intradepartmental Viral Infection Unit, Sagol School of Neuroscience, Tel Aviv University, Tel Aviv 6997801, Israel; meishars@mail.tau.ac.il

⁴ Department of Statistics and Operations Research, School of Mathematical Sciences, Raymond and Beverly Sackler Faculty of Exact Sciences, Tel Aviv University, Tel Aviv 6997801, Israel; jaljuli.iman@gmail.com

⁵ The Myers Neuro-Behavioral Core Facility, Sackler School of Medicine, Tel Aviv University, Tel Aviv 6997801, Israel; liorbiko@gmail.com

⁶ Department of Neurology and Neurological Sciences, Stanford University School of Medicine, Stanford, CA 95343, USA; palovics@stanford.edu (R.P.); tal.iram8@gmail.com (T.I.)

⁷ Wu Tsai Neurosciences Institute, Stanford University School of Medicine, Stanford, CA 95343, USA

* Correspondence: igozes@tauex.tau.ac.il; Tel.: +03-6407240

Received: 22 September 2020; Accepted: 15 October 2020; Published: 19 October 2020



Abstract: Activity-dependent neuroprotective protein (ADNP) mutations are linked with cognitive dysfunctions characterizing the autistic-like ADNP syndrome patients, who also suffer from delayed motor maturation. We thus hypothesized that ADNP is deregulated in versatile myopathies and that local ADNP muscle deficiency results in myopathy, treatable by the ADNP fragment NAP. Here, single-cell transcriptomics identified *ADNP* as a major constituent of the developing human muscle. *ADNP* transcript concentrations further predicted multiple human muscle diseases, with concentrations negatively correlated with the ADNP target interacting protein, microtubule end protein 1 (EB1). Reverting back to modeling at the single-cell level of the male mouse transcriptome, *Adnp* mRNA concentrations age-dependently correlated with motor disease as well as with sexual maturation gene transcripts, while *Adnp* expressing limb muscle cells significantly decreased with aging. Mouse *Adnp* heterozygous deficiency exhibited muscle microtubule reduction and myosin light chain (*Myl2*) deregulation coupled with motor dysfunction. CRISPR knockdown of adult gastrocnemius muscle *Adnp* in a Cas9 mouse resulted in treadmill (male) and gait (female) dysfunctions that were specifically ameliorated by treatment with the ADNP snippet, microtubule interacting, *Myl2*—regulating, NAP (CP201). Taken together, our studies provide new hope for personalized diagnosis/therapeutics in versatile myopathies.

Keywords: muscular dystrophy; neuromuscular diseases; ADNP; NAP; CRISPR/Cas9

1. Introduction

Essential for brain formation, activity-dependent neuroprotective protein (ADNP) [1–3] is a major brain regulatory gene [4]. *De novo* mutations in *ADNP* result in the *ADNP* syndrome, with children suffering from severe global developmental delays that affect the central and peripheral nervous systems [5]. Several structural abnormalities in the *ADNP* syndrome brain were observed including cerebral atrophy, delayed myelination, white matter lesions, and wide ventricles [5,6]. Other pathological outcomes include impairments in motor function, delayed speech acquisition, intestinal and urinary problems [5,7] as well as early tooth eruption [8]. Thus, *ADNP* mutations affect the three germ layers during development [9].

Using quantitative RT-PCR we have recently shown that *Adnp*^{+/-} heterozygous deficiency in mice resulted in aberrant gastrocnemius muscle, tongue, and bladder gene expression, which was corrected by the ADNP fragment, drug candidate, NAP (CP201) [10]. A significant sexual dichotomy was revealed, coupled to muscle and age-specific gene regulation. Thus, *Adnp* regulated myosin light chain (*Myl*) transcript in the gastrocnemius muscle, the language acquisition gene forkhead box protein P2 (*Foxp2*) transcript in the tongue muscle, and the pituitary adenylate cyclase-activating polypeptide (PACAP) receptor PAC1 mRNA (*Adcyap1r1*) in the bladder, with PACAP, linked to bladder function [11] and partly controlling *Adnp* expression [12]. A sex-dependent *Adnp*-regulated gene transcript correlation to gait patterns (CatWalk) was discovered, placing ADNP as a muscle-regulating gene/protein [10].

We have also previously shown that the expression levels of *ADNP* and its paralogue protein *ADNP2* in the vastus lateralis and biceps brachii muscles are sex-dependently upregulated in elderlies compared to young subjects [13]. The *ADNP* transcript displayed age-dependent correlations with 49 muscle gene transcripts. Among these 49 transcripts, *ADNP* expression was highly correlated with 24 transcripts, singling nicotinamide nucleotide adenylyl (NAD) transferase 1 (*NMNAT1*) as the leading gene/protein [13]. Importantly, the *NMNAT1*-associated regulation of NAD⁺ salvage capacity in human skeletal muscle is declining with aging, while aerobic and resistance training attenuate this decline [14]. Thus, ADNP is implicated in human muscle aging.

A similar association of ADNP with aging has been suggested in the Alzheimer's brain, with the observed correlation between somatic ADNP mutations and increased Alzheimer's Tau pathology [13], directly linked to ADNP's function as enhancing Tau-microtubule interaction [15].

Mechanistically, ADNP, a double-edged sword, is found in the cell nucleus and the cytoplasm [16]. In the nucleus, ADNP binds DNA, acting as a transcription factor [2,17], taking part in chromatin remodeling/epigenetic modifications [17–19] as well as RNA splicing interactions [20]. In the cytoplasm, ADNP binds the autism-linked eukaryotic initiation factor 4E (eIF4E) [21,22] and regulates microtubule dynamics by binding to the microtubule end binding proteins EB1 and EB3 [23], further enhancing Tau-microtubule interaction [15,24]. Microtubule function is sexually-dependent and *Adnp* deficiency results in reduced axonal transport [25]. The major cellular autophagy pathway is dependent on microtubule integrity [26], and ADNP also binds the microtubule-associated protein 1 light chain 3B (MAP1LC3B). Importantly, LC3 is a major protein forming the autophagosome [27]. ADNP binding to LC3 and EB1/EB3 is enhanced in the presence of NAP (NAPVSIPQ, drug candidate CP201) containing an EB1/EB3 and self-interacting SxIP motif [15,24–27].

Given the significant effect of ADNP mutations and ADNP deficiency on motor functions [28], we hypothesized that it is involved with versatile muscle diseases. Table S1 summarizes muscle diseases that may entwine with ADNP function including association with the cytoskeleton/microtubules, autophagy, and aberrant gene regulation. In short, these diseases may include myotonic dystrophy (e.g., DM2) [29], Duchenne muscular dystrophy (DMD) [30,31], Becker muscular dystrophy (BMD) [32,33], Pompe disease [34], tibial muscular dystrophy (TMD) [35], dysferlinopathy [36], secondary dystroglycanopathies [37] and amyotrophic lateral sclerosis (ALS) [38].

Taking advantage of single-cell transcriptomic data in humans and mice, we were able to show the developmental expression of ADNP in human muscle progenitor cells and correlate muscle disease

genes with *Adnp* in mice. Modeling *Adnp* deficiency in mice, we further asked whether such deficiency was linked to muscle regulation. Lastly, we investigated if Cas9-mediated muscle-specific adult mouse *Adnp* knockdown resulted in motor deficiencies, which could be significantly reversed by NAP treatment.

2. Materials and Methods

2.1. Human Muscle Single Cell Data Mining

The NCBI GEO website was screened for datasets derived from human single-cell transcriptomes of skeletal muscles. In the dataset GSE147457 [39] human tissues including hind limbs of developmental weeks 5–18 human embryos and fetuses, and gastrocnemius or quadriceps muscles from juvenile and adult human were processed into single cells. The UCSC Cell Browser [40] was used to analyze the data. 2D plots of single cells were visualized by the t-SNE algorithm, and ADNP expressing cells were marked in black. The expression levels of ADNP in developmental weeks 5–18, years 7, 11, 34, and 42 were downloaded from UCSC single-cell browser. Average expression levels for each cell type and time point were calculated, and the dot plot figure was generated with Tableau 2019.2 software. The Violin plots were generated for cells expressing ADNP, DMD, GAA, and DYSF with ggplot, RStudio Version 1.2.5033 (RStudio, PBC, Boston, MA, USA).

2.2. Online Gene Expression Omnibus (GEO) Public Functional Genomics Data Repository, Human Muscle Diseases

A summary of the different patients and age-matched controls is presented in Table S2, Specific datasets included GAA, GSE38680 [41], GSE1007 [42], GSE45331 [43], GSE42806 [43] and GSE3307 [44,45].

2.3. Secondary Analysis of Tabula Muris Senis Single-Cell Data Set

Raw cell-to-gene count matrix along with sample metadata was acquired from AWS using project ID arn:aws:s3:::czb-tabula-7 muris-senis. Here, the FACS Smart-seq2 data uploaded on 12 April 2019 was analyzed. To minimize possible sources of bias, female cells, which had lower coverage across cell types and time points, were excluded from subsequent analysis. Cells with either less than 500 genes detected or 50,000 reads in total were removed from the expression matrix. Counts were then normalized as $\log(\text{CPM} + 1)$. To visualize the cell-type clusters we computed t-SNE embeddings over the 16 principal components of the normalized expression matrix. The similarity between the expression of all detected genes and *Adnp* was calculated based on the cosine similarity. All computational steps were done by using Python with the packages Scanpy v1.4.4, Pandas v1.0.1, Numpy v1.18.1, and Scikit-learn v0.22.1 (DataCamp, New York, NY, USA).

2.4. Animals

All procedures were approved by the IACUC of Tel Aviv University and the Israeli Ministry of Health (01-18-020; 01-18-018).

Two mouse models were used:

(1) The *Adnp*^{+/-} mice, on a mixed C57BL and 129/Sv background [4,21,28,46,47], outbred with an ICR mouse line for continuous breeding [21,25].

(2) Cas9 expressing Gt(ROSA)26Sor^{tm1.1(CAG-cas9*, -EGFP) F₀zh} (Jackson Laboratory, stock: 024858) males crossbred with female ICR mice and progeny subjected to muscle *Adnp* knockdown (Cas9 mice, below).

2.4.1. Neuromuscular Junction (NMJ) Staining

Medial gastrocnemius muscles were excised from 7-month-old and 14-month-old *Adnp*^{+/-} male mice and stained as before [48,49]. Digital images were obtained using a Leica SP5 confocal laser scanning microscope [48].

2.4.2. Peptide Synthesis and Formulations

NAP was custom synthesized and formulated as before [28,50–52]. Specifically, NAP was dissolved in a vehicle solution termed DD, in which each milliliter included 7.5 mg of NaCl, 1.7 mg of citric acid monohydrate, 3 mg of disodium phosphate dihydrate, and 0.2 mg of benzalkonium chloride solution (50%). A second vehicle solution termed CB included 0.25% chlorobutanol, 0.85% NaCl, pH = 3.5 to 4.0. On days of scheduled behavioral tests, NAP was applied 2 h before the behavioral tests.

2.4.3. RNA Extraction and Quantitative Real-Time PCR

Adnp^{+/-} mice were divided into groups and sacrificed for RNA extraction by the end of the treatment period. All behavioral assessments and RNA extractions (TRI Reagent, T9424, Sigma-Aldrich, Jerusalem, Israel) and gene expression analysis were carried out before as described before in a semi-blinded manner [28,51] and correlated with gene expression results. RNA expression levels were determined using specific mouse primers: *Adnp* sense 5'-ACGAAAATCAGGACTATCGG-3', anti-sense 5'-GGACATTCCGGAAATGACTTT-3', *Myl2* sense 5'-GCCCTAGGACGAGTGAA-3', anti-sense 5'-CCAAACATCGTGAGGAAC-3'. mRNA levels were normalized to *Hprt* sense 5'-GGATTGAATCACGTTTGTGTC-3', anti-sense 5'-AACTTGCGCTCATCTTAGGC-3'. Results are presented as 2^{-ΔCT} [53].

Muscle *Adnp* knockdown Cas9 mice were treated daily throughout the experiment (0.5 μg intranasal NAP/5 μL DD per mouse) and subjected to behavioral experiments (below).

2.4.4. Vially-Delivered CRISPR-Mediated *Adnp* Knockdown in Muscle Tissue of Cas9 Mice: Cell Lines for Reagent Preparations

NIH 3T3 cells, mouse fibroblasts, and HEK-293T, human embryonic kidney cell lines (ATCC), were plated in DMEM supplemented with 10% fetal calf serum, 2mM glutamine, and 1% penicillin-streptomycin (Biological Industries, Beit HaEmek, Israel) [17]. The cells were incubated in 95% air/5% CO₂ in a humidified incubator at 37 °C.

2.4.5. Single Guide RNA (sgRNA) Preparation and Plasmid Construction

Three different sgRNA were designed using CRISPOR [54]. To determine the effectivity of the designed *Adnp* sgRNAs (targeting the second coding exon (exon No.4) of *Adnp*), NIH 3T3 cells (ATCC) were transfected in triplicates with PX459 plasmids (Addgene #62988, from Feng Zhang, Broad Institute, MIT and Harvard, Cambridge, MA, USA) [55], encoding three different *Adnp* sgRNA (termed 60,67,68) and an empty plasmid as a control using jetPEI (101-10N, Polyplus Transfection, Illkirch, France). Transfected cells were selected using 3 μg/mL Puromycin (P7255, Sigma-Aldrich) for two weeks. Extracted total cellular protein was subjected to Western blotting [24] and ImageJ software quantification (NIH, Bethesda, MD, USA) [15].

2.4.6. Lentivirus Production and Injection

Lentiviral vectors were generated by insertion of the guide-RNA sequences, SgRNA 68 and a stuffer (poly T), into the third generation lenti backbone pAW13.lentiguide.mCherry (Addgene #104375, a gift from Richard Young, MIT, Cambridge, MA, USA) [56]. High-titer lentiviral stocks pseudo-typed with the vesicular stomatitis virus G protein (VSV-G) were produced in HEK293T cells [57,58]. 3-month-old Cas9-expressing male and female mice were anesthetized using isoflurane. Next, 100 μL of Neurobasal medium containing lentiviruses at a concentration of 2.96 × 10⁷ titer

units, expressing either G68 (knocking down the *Adnp* gene) or Poly T (stuffer) were injected into gastrocnemius muscles, using a 1 mL syringe and a 25G needle. Each virus was injected into both hind limbs of the same animal. Animal group sizes were determined in a pilot study. Cas9 mice from five litters were included in the study and randomly divided into four different groups, per sex as follows: (1) Injection control group (NB) (male $n = 4$; female $n = 4$), (2) PolyT DD (male $n = 12$; female $n = 8$), (3) G68 DD (male $n = 7$; female $n = 7$), (4) G68 NAP (male $n = 8$; female $n = 7$).

2.4.7. Behavioral Studies

A month following viral injections and NAP or DD daily treatments, male and female Cas9 mice were subjected to multiple behavioral tests.

2.4.8. Gait Analysis

CatWalk XT (Noldus Information Technology, Wageningen, The Netherlands) was used [28,59,60].

2.4.9. Treadmill

The treadmill apparatus (Panlab, Harvard Apparatus, Barcelona, Spain) was used [61].

2.4.10. Hot plate

The hot plate (Ugo Basile, Gemonio VA, Italy) was used [62].

2.5. Statistics

Results were analyzed for statistical significance using (1) Sigma Plot for Windows software version 11 (Chicago, IL, USA) and (2) R Core Team (2019) for Mac, version 3.6.2 (2019-12-12) (R Foundation for Statistical Computing, Vienna, Austria). The analyses and graphs produced by R were performed using the libraries: lme4, lmerTest, and ggplot2. The reported estimators of effects and differences in pairwise comparisons were obtained by the Restricted Maximum Likelihood (ReML) method.

The models used for data analyses were one- or two-way ANOVA and logistic regression mixed-effects as detailed below. Statistical significance of the pairwise comparisons was evaluated by the model-corresponding post-hoc t-test, with correction multiple comparisons. Sex differences were revealed between male and female mice using an unpaired Student's t-test.

Inclusion/exclusion of values per each tested group were performed using Grubbs' test. All determinations were considered to be statistically significant at the $p < 0.05$ level: * $p < 0.05$, ** $p < 0.01$, *** $p < 0.001$.

3. Results

3.1. Human Single Cell ADNP Is Increased in Single Muscle Progenitor Cells

To place ADNP transcript expression directly in human muscle cells, we resorted to whole-cell transcriptomics. We used an available dataset (GSE147457). As previously published, whole hind limbs of developmental week 5–9 human embryos and fetuses (feet excluded for week 7.75–9), total hind limb skeletal muscles of week 12–18 human fetuses, and gastrocnemius or quadriceps muscles from juvenile and adult human subjects were digested into single cells. Dissociated cells were either sorted (fetal week 12 and above) to exclude the hematopoietic and endothelial lineages or directly used for downstream processing [39]. Figure 1A shows single-cell *ADNP* transcriptomes of skeletal muscles, gastrocnemius, and quadriceps muscles from human specimen ranging from 5-week-gestation to 42 years of age. Results indicated increased expression in the young embryonic muscle. Figure 1B focuses on 9-day gestation hind limb cells indicating enrichment of *ADNP* in pre-chondrocytes and skeletal muscle cells, showing expression in dividing cells of the myogenic subset myogenic progenitor cells (inset). Figure S1 details cellular expression at 12–14 and 17–18 weeks of gestation,

respectably, with skeletal muscle at all stages, and with mesenchymal stromal cells increasing at 12–14-gestational-weeks and further increasing at 17–18-gestational-weeks.

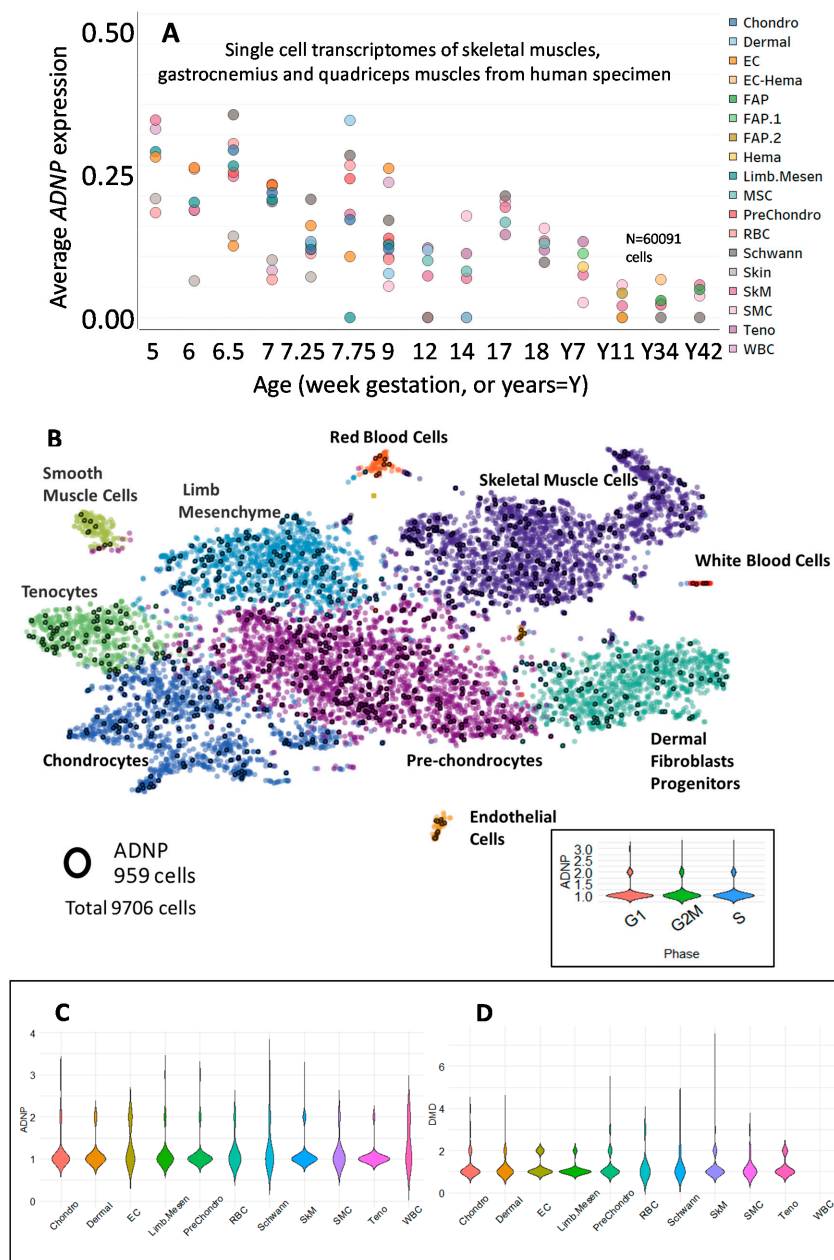


Figure 1. ADNP is expressed in the single human muscle cell. Single-cell transcriptomes of skeletal muscles, gastrocnemius, and quadriceps muscles from a human specimen (GEO dataset GSE147457). (A) Average expression levels of ADNP for each cell type and through developmental weeks 5–18 and years 7, 11, 34 42. $n = 60,091$ cells. (B) ADNP-expressing cells are marked in black-2D plots of single cells, visualized by the t-SNE algorithm, UCSC Cell Browser [40]. Inset: Violin plot of ADNP expression levels in single cells in phases G1, G2M, and S. $n = 9706$ cells. (C,D) Violin plots of single-cell expression levels of ADNP and DMD in each cell type. Chondro = Chondrocytes, Dermal = Dermal Fibroblasts Progenitors, EC = Endothelial Cells, EC-Hema = Endothelial, and Hematopoietic Cells, FAP = Fibro-adipogenic Progenitor, Hema = Hematopoietic Cells, Limb. Mesen = Limb Mesenchyme, MSC = Mesenchymal Stromal Cells, PreChondro = Pre-chondrocytes, RBC = Red Blood Cells, Schwann, SkM = Skeletal Muscle Cells, SMC = Smooth Muscle Cells, Teno = Tenocytes, WBC = White Blood Cells [39].

3.2. ADNP Expression Plays a Role in Childhood and Adult-Onset of Neuromuscular Disorders

Figure 1C,D depict violin single-cell expression graphs at the 9-gestational week of ADNP and dystrophin (DMD), a major neuromuscular disease gene, as an example (Table S1), indicating some similarities. Given the potential parallelism between ADNP and the expression of DMD as well as other gene transcripts representatives of muscle disease (Figure S2), it was of interest to address the question if ADNP expression is altered in neuromuscular disorders. Thus, the online Gene Expression Omnibus (GEO) public functional genomics data repository was searched for expression datasets of human subjects afflicted with various neuromuscular disorders, comparing transcriptional profiles of controls and affected individuals. A summary of the different patients and age-matched controls is presented in Table S2, indicating specific muscle sampled and sex. Interestingly, microarray expression levels of ADNP in different muscle types showed significant downregulation in four out of the eight tested neuromuscular disorders including Pompe, caused by mutations in the acid alpha-glucosidase (GAA, GSE38680) [41] (sampled tissue, biceps), Duchenne muscular dystrophy caused by dystrophin (DMD) absence (GSE1007) [42], (quadriceps-vastus lateralis), myotonic dystrophy type 2 (DM2), caused by mutations in the cellular nucleic acid-binding protein gene, CNBP (GSE45331) [43] (vastus lateralis), and tibial muscular dystrophy (TMD) caused by mutations in titin (TTN, GSE42806) [43] (distal muscles), compared with healthy controls (Figure 2A–D). Further analysis of the GEO data set GSE3307 [44,45] showed significant increases in the expression levels of ADNP in the vastus lateralis of other muscle pathologies including Becker muscular dystrophy (BMD, DMD mutations), dysferlin mutation (DYSF) [63], fukutin-related protein (FKRP) mutation [64] and amyotrophic lateral sclerosis (ALS), compared with matched healthy controls (Figure 2E,F). We were also interested in whether each of these eight diseases can be anticipated by ADNP expression levels. In Pompe, DM2, TMD, and BMD patients, ADNP expression values essentially did not intersect with control values; therefore, the rule of differentiation is quite clear, not requiring statistical modeling. For the other tested diseases (DMD, FKRP, DYSF, and ALS) with extensive overlapping values, we performed logistic regressions estimating the probability of disease diagnoses via ADNP levels. Results showed significantly predictive values (Figure 2G). The tendency to develop each of the illnesses, for any given expression level was predicted by logistic regression. To draw a differentiating line between expression levels with high risk, we used the default probability cutoff, 0.5. Explicitly, expression levels that were accompanied by the probability of illness that was over 50% (dashed vertical lines) were classified as indicators of future diagnosis (Figure 2G).

Given the dichotomous downregulation versus the upregulation of ADNP in the different diseases, we examined also the ADNP cytoplasmic targets EB1 and EB3 also called microtubule-associated protein RP/EB family member 1 (MAPRE1) and MAPRE3. We thus discovered that MAPRE1 and to a lesser extent MAPRE3 are regulated in an opposite way compared to disease-downregulated ADNP (Figure 2A–C). Specifically, both MAPRE1 and MAPRE3 were upregulated in Pompe disease (Figure 2A), and MAPRE1 was upregulated in DM2, TMD, and DMD (Figure 2B,C,H). In contrast, in ALS and BMD, MAPRE3 expression did not differ between control and disease, and MAPRE1 was increased (Figure 2H). In DYSF and FKRP, no significant differences were found for MAPRE1 or MAPRE3 between controls and disease afflicted subjects. Individual correlations showed a highly significant negative correlation between MAPRE3 and ADNP expression in Pompe disease (Figure 2A, $r = -0.781$, $*** p < 0.001$, Spearman). A similar correlation was found in TMD for MAPRE1 and ADNP (Figure 2C, $r = -0.620$, $*p = 0.0315$, Pearson). Lastly, in ALS, a positive correlation was discovered between the expression of MAPRE1 and ADNP (Figure 2F,H $r = +0.601$, $*** p < 0.001$, Spearman).

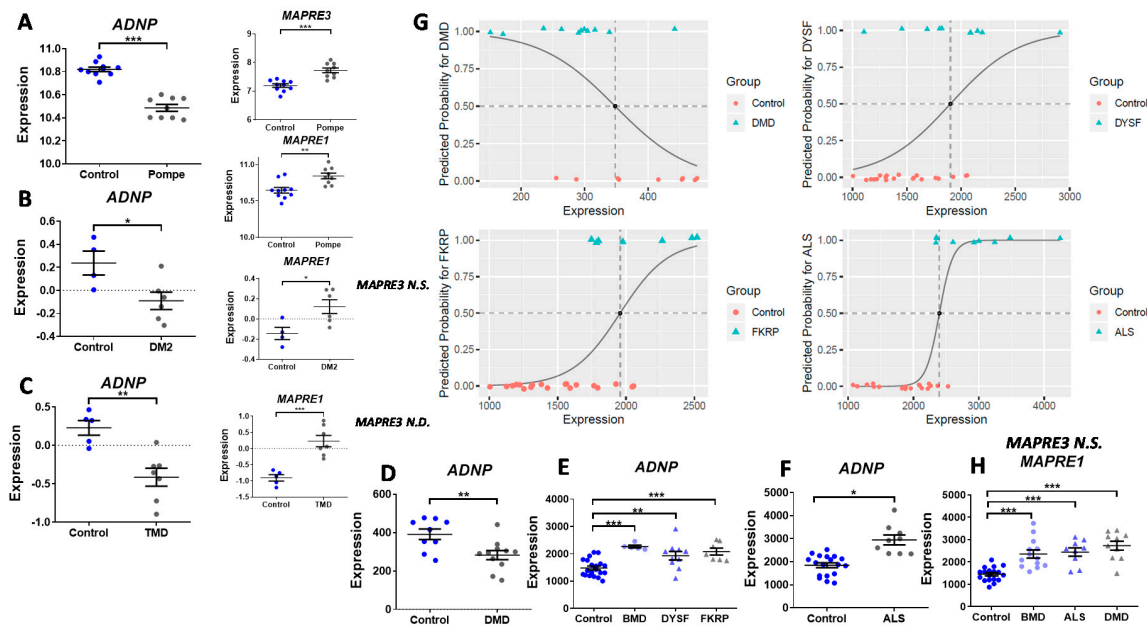


Figure 2. *ADNP* is dysregulated in different neuromuscular disorders. (A–D) *ADNP* was significantly downregulated in various muscle types: bicep, quadriceps, vastus lateralis and distal muscles from patients with a range of neuromuscular disorders: Pompe $n = 9$ (control $n = 10$, GSE38680), DMD $n = 11$ (control $n = 11$, GSE1007), DM2 $n = 6$ (control $n = 4$, GSE45331) and TMD $n = 7$ (control $n = 5$, GSE42806), as revealed by two-tailed Student’s *t*-test ($* p < 0.05$, $** p < 0.01$, $*** p < 0.001$, and $** p < 0.01$, respectively). (A–C) *MAPRE3* was upregulated in Pompe disease and *MAPRE1* was upregulated in Pompe, DM2 and TMD, in the same subjects/tissues as above (N.S. insignificant, N.D. not determined). (E,F) *ADNP* was significantly upregulated in microarray expression levels of vastus lateralis muscle biopsy specimens from patients with various muscle diseases: control ($n = 20$), BMD ($n = 5$), DYSF ($n = 10$), FKRP ($n = 7$) (data set GSE3307, U133B Array), ALS ($n = 9$) (data set GSE3307, U133A Array). One-way ANOVA followed by a Tukey post hoc test (for GSE3307, U133B Array) or Dunn’s Method (for GSE3307, U133A array, due to Equal Variance Test Failed) was performed using SigmaPlot ($* p < 0.05$, $** p < 0.01$ and $*** p < 0.001$, respectively). (G) Logistic regression was performed to estimate the probability of disease diagnoses via *ADNP* levels. DMD; the model estimates a 1.7% decrease in odds of disease, where OR = 0.983, $\text{pv}(\text{chisq}(\text{DF} = 1) > 4.873) = 0.027$, $\text{CI}(95\%) = [0.968, 0.998]$, AUC = 0.818. DYSF; the model estimates an increase of one unit in “expression” increases the odds for DYSF by 0.3%, where OR = 1.003, $\text{pv}(\text{chisq}(\text{DF} = 1) > 5.604) = 0.018$, $\text{CI}(95\%) = [1.001, 1.006]$, AUC = 0.805. FKRP mutation; the model estimates an increase of one unit in expression increases the odds for FKRP by 0.6%, where OR = 1.006, $\text{pv}(\text{chisq}(\text{DF} = 1) > 5.799) = 0.016$, $\text{CI}(95\%) = [1.001, 1.010]$, AUC = 0.9. ALS; the model reports an increase one unit in expression increases the odds for ALS by 1%, where OR = 1.010, $\text{pv}(\text{chisq}(\text{DF} = 1) > 3.403) = 0.065$, $\text{CI}(95\%) = [0.999, 1.02]$, AUC = 0.963. (H) *MAPRE3* did not change in BMD, ALS and DMD, *MAPRE1* was significantly increased, please see D–F for further description of the samples.

3.3. Mouse Single Cell Analysis Age-Dependently Correlates *Adnp* to Muscle Disease Genes

Although correlation is not causation, we were interested in correlating *Adnp* gene transcript concentrations to muscle disease genes at the single-cell level [13,65,66]. We resorted to data mining of two libraries, the young (3-month-old) and the aged (18 and 24 months) male mice, and focused on 8 genes as illustrated in Table 1. For each of the genes, we showed the cell type exhibiting the highest correlation to *Adnp* (see methods), in young mice, and further showed that these correlations were mostly lost in aged mice. Surprisingly, the tissue origin of the cells showing the highest correlative values were the brown adipose tissue, the pancreas, the large intestine, and the lung, possibly implicating *Adnp* and muscle disease genes in functions beyond the neuromuscular junction (NMJ). Only *Fkrp* (associated with adherence to the extracellular matrix, Table S1) remained correlated with *Adnp* in the aging bronchial smooth muscle cell.

Table 1. *Adnp* correlates with muscle disease gene transcripts at the single-cell level. Cosine similarity values for the genes of interest (see Gene) and *Adnp* in young (3 months) and aged (18 and 24 months) mouse tissue and cell types at the single-cell level, showing an overall loss of correlation with *Adnp* with aging.

Cell type	Brown Adipose		Pancreas		Large Intestine		Lung	
	Mesenchymal stem cell	Endothelial cell	Polypeptide cell		Goblet cell	Epithelial cell	bronchial smooth muscle cell	
Gene	<i>Dmd</i>	<i>C9orf72</i>	<i>Cnbp</i>	<i>Fkrp</i>	<i>Ttn</i>	<i>Gaa</i>	<i>Fkrp</i>	<i>Dysf</i>
<i>Adnp</i> correlation (young)	0.539	0.643	0.547	0.402	0.392	0.545	0.577	0.383
<i>Adnp</i> correlation (old)	0	0	0	0	0	0	0.497	0

At the general limb muscle level, most of the disease genes in which *ADNP* reduction was disease predictive correlated with *Adnp* expression in the young specimens. *Cnbp* seemed relatively highly correlated with *Adnp*, associated with the most common adult myotonic dystrophy, DM2, (Table S1), while *Ttn* showed almost no correlation (Figure 3). Of note, for ALS, we have used *C9orf72*, which most certainly does not represent all cases of sporadic ALS.

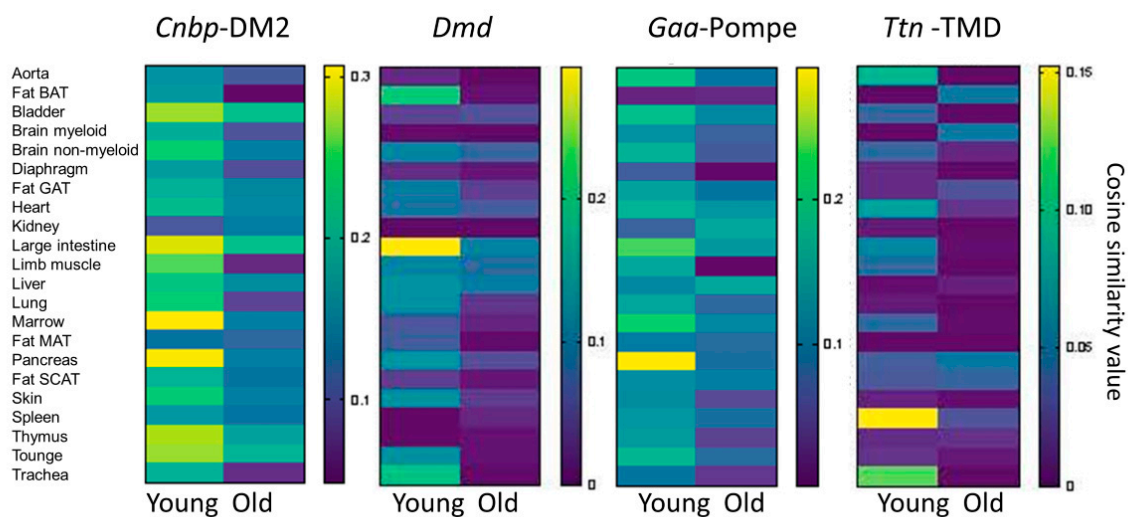


Figure 3. Correlation of *Adnp* and muscle disease genes in the single-cell/general tissue. Heatmaps plotting cosine similarity values (indicating co-expression at the single-cell level) for the genes of interest (indicated above each heatmap) and *Adnp* in young (3 months) and aged mice (18 and 24 months) in 22 tissues (indicated in rows). GAT, SCAT, MAT, and BAT stand for gonadal-, subcutaneous-, mesenteric- and brown-adipose tissue.

Furthermore, genes in which reduction in *ADNP* was disease predictive (Figure 2), showed apparent higher *Adnp* correlations compared to genes in which increases in *ADNP* correlated with the disease (Figure 3 vs. Figure S3, respectively). The correlations were reduced with aging (Figure 3) with disease genes associated with *ADNP* increases, completely losing correlation with aging (Figure S3).

In general, searching for genes with the highest correlative expression to *Adnp* at the cellular level, we discovered in the young male mouse (and not in the aged mouse), a 0.9 correlation with the gonadotropin-releasing hormone receptor (*Gnrhr*) transcript in diaphragm mesenchymal stem cells, tying *Adnp* to sexual maturation, with muscle diseases being highly sexually dichotomized (Table S1).

Overall cell-specific age and sex-dependent expression (male) patterns of *Adnp* were observed (Figure 4A), with significant differences marked with asterisks. In most tissue-representing cells, *Adnp* expression, and/or the fraction of cells expressing *Adnp* significantly decreased with aging,

except for liver, aorta, and mesenchymal fat, showing low expression levels (Figure 4A). To evaluate mouse *Adnp* age-dependent expression in limb muscle cell types (Figure 4B), we specifically looked at the single-cell level where *Adnp* is found in various limb muscle cell types (see blue dots in Figure 4C) with a significant decrease in *Adnp* positive cells remaining in aged muscle (red dots in Figure 4D).

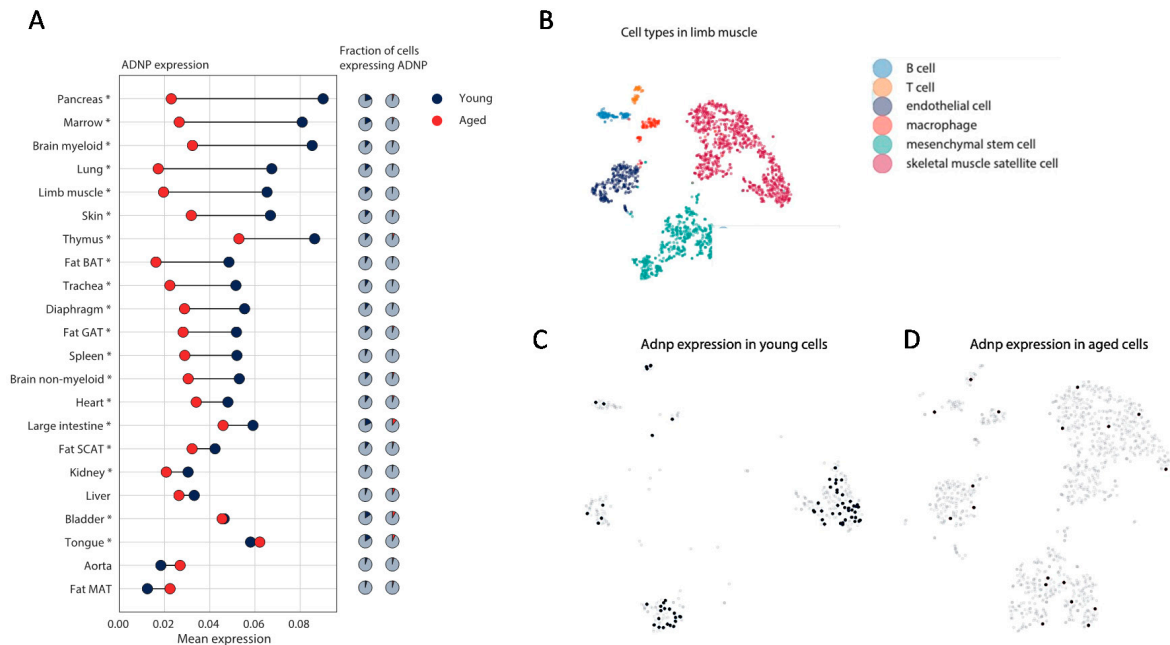


Figure 4. *Adnp* expression is downregulated with age, specifically in limb muscle cells. (A) Mean *Adnp* expression in young (3 months) and aged mice (18 and 24 months) in 22 tissues (indicated in rows). GAT, SCAT, MAT and BAT stand for gonadal-, subcutaneous-, mesenteric- and brown-adipose tissue. Asterisk indicates * $p < 0.05$ using the Wilcoxon rank-sum test. (B) Annotated cell type clusters in the limb muscle tissue. (C) Out of 542 limb muscle cells in the young mouse 70 express *Adnp* (overlaid as dark blue dots). (D) Out of 1315 limb muscle cells in the aged mouse 18 express *Adnp* (overlaid as light blue dots).

3.4. *Adnp*^{+/-} Mice Display Neuromuscular Junction (NMJ) Disruption, Significantly Correlated with Behavioral Deficits

To further evaluate the mechanistic role of ADNP in muscle function, we utilized muscle histochemistry and gene expression measurements in *Adnp*^{+/-} mice.

Adnp^{+/-} mice treated with the intranasal formulation chlorobutanol (CB), serving as controls for future drug studies (employing the CB formulation), were previously used [51]. Here, representative whole-mount NMJ staining of the gastrocnemius muscle obtained from 7-month-old CB-treated *Adnp*^{+/+} and *Adnp*^{+/-} male mice are shown (Figure 5A). Sections were labeled with the post-synaptic marker α -bungarotoxin (BTX) and the pre-synaptic marker tubulin (TUB 2.1 monoclonal antibodies) [48,49,51]. Results indicated significantly decreased tubulin intensities in *Adnp*^{+/-} vs. *Adnp*^{+/+} muscles (Figure 5A, reduction of 21.5%). We have repeated and extended this result in muscles from 14-month-old mice showing a 32.3%-genotype related reduction in tubulin staining (Figure S4).

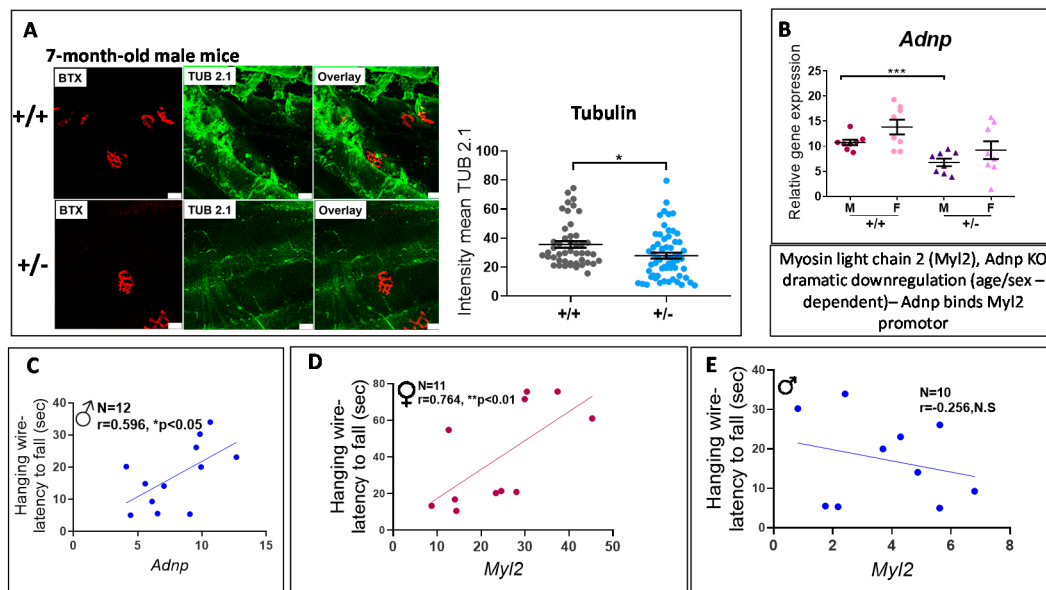


Figure 5. NMJ disruption in the gastrocnemius muscle of *Adnp*-deficient mice correlates behavior. (A) Representative whole-mount NMJ immunostaining of 7-month-old (*Adnp*^{+/+} CB n = 4; *Adnp*^{+/-} CB n = 4) male mice. The post-synaptic marker nicotinic acetylcholine receptor was labeled by bungarotoxin (BTX, red) and the pre-synaptic marker tubulin was labeled by TUB 2.1 (green). Decreased tubulin intensity was observed in *Adnp*^{+/-} CB, compared with *Adnp*^{+/+} CB, (* p < 0.05). The images were acquired by a confocal microscope at ×20 magnification. Scale bar 25 μm. (B) qRT-PCR analysis was performed on mRNA extracted from gastrocnemius muscle of 7-month-old male and female mice (Males: *Adnp*^{+/+} CB n = 4, *Adnp*^{+/-} CB n = 4; Females: *Adnp*^{+/+} CB n = 4, *Adnp*^{+/-} CB n = 4). Results were normalized to hypoxanthine-guanine phosphoribosyltransferase (*Hprt*). In males, an unpaired Student's t-test revealed significant differences between CB-treated *Adnp*^{+/+} and *Adnp*^{+/-} mice (*** p < 0.001). Significant correlations were observed between behavioral tests (Hanging wire) and gene expression (*Adnp* C, *Myl2* D,E) results in 7-month-old mice. Correlative analyses were performed using either the Pearson correlation coefficient method or the Spearman's rank correlation coefficient if at least one of the data sets was not normally distributed. Male significant correlations are presented in blue and female significant correlations are presented in magenta.

Quantitative real-time PCR (qRT-PCR) assays evaluating *Adnp* mRNA expression were further performed on RNA extracted from gastrocnemius muscles of CB-treated 7-month-old male and female mice (*Adnp*^{+/+} and *Adnp*^{+/-}). A significant genotype-related reduction was observed in males (Figure 5B), but not in females. Most importantly, significant positive correlations were discovered between behavioral test results (hanging wire, measuring the latency to fall off an inverted cage lid [51]) and gene expression levels (*Adnp*) in muscles of 7-month-old mice (Figure 5C). Further hanging wire behavioral correlations were discovered with myosin light gene 2 (*Myl2*), a major gene regulated by *Adnp* [9,25] in a sex-dependent manner (Figure 5D,E).

To further substantiate the mechanistic basis for the effects of ADNP in relation to *Myl2* on muscle development/function, we examined the water-based DD-formulated/NAP-treated *Adnp*^{+/-} and *Adnp*^{+/+} mice, extensively studied for brain function and behavior before (methods) [28]. Thus, we assessed *Adnp* and *Myl2* gene expression patterns in the gastrocnemius muscle in correlation with behavior in 19–27-days-old mice.

Adnp reduction as a consequence of *Adnp* gene copy deficiency (*Adnp*^{+/-}) was significant in both males and females, coupled with higher expression of *Adnp*^{+/+} males compared with females. *Myl2* showed the opposite expression pattern, being higher in *Adnp*^{+/+} females, significantly reducing with *Adnp* deficiency in females only, and normalized by the ADNP snippet NAP treatment (Figure 6A).

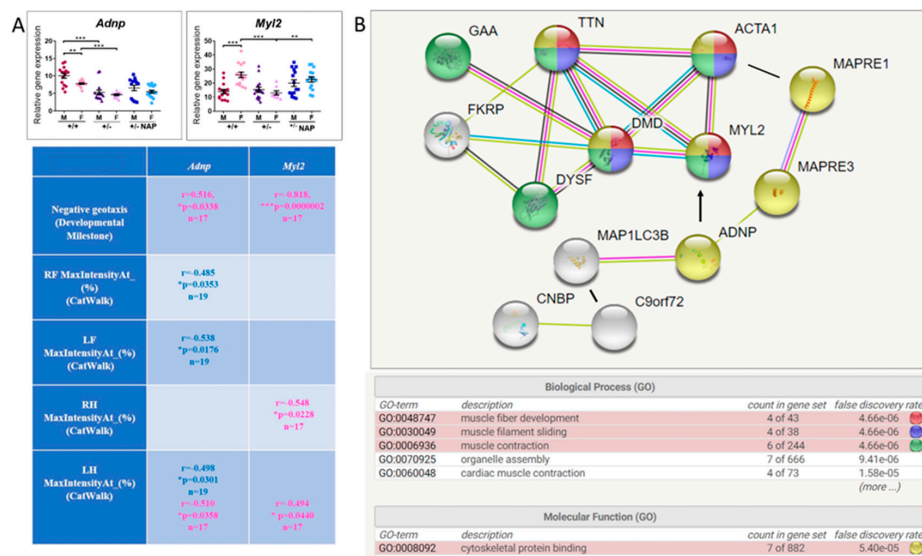


Figure 6. *Adnp* and the *Adnp*-regulated *Myl2* correlate with muscle function and behavior. (A) Gastrocnemius muscle total RNA was extracted from 19–27-day-old mice (males: *Adnp*^{+/+} $n = 5$, *Adnp*^{+/-} $n = 5$, *Adnp*^{+/+} NAP $n = 4$, *Adnp*^{+/-} NAP $n = 5$; females: *Adnp*^{+/+} $n = 5$, *Adnp*^{+/-} $n = 3$, *Adnp*^{+/+} NAP $n = 4$, *Adnp*^{+/-} NAP $n = 5$). Results were normalized to *Hprt*. A two-way ANOVA with Tukey’s post hoc test revealed significant differences between vehicle-treated *Adnp*^{+/+} and *Adnp*^{+/-} mice and between NAP and vehicle-treated *Adnp*^{+/-} mice (** $p < 0.01$ and *** $p < 0.001$). Sex differences were determined by unpaired Student’s *t*-test. (B) STRING analysis [67] was performed as described in the text, with human muscle disease proteins delineated in Figure 2 and Table 1 and Table S1. Additional proteins included muscle actin (ACTA1), the ADNP/NAP-binding EB1 (MAPRE1), and EB3 (MAPRE3) and MAP1LC3B as well as the ADNP/NAP-regulated MYL2.

We also correlated *Adnp* and *Myl2* expression levels with previously published behavioral outcomes [28] and significant results are depicted in the Table insert in Figure 6A. In short, both *Adnp* and *Myl2* highly correlated with the first day of acquisition of the negative geotaxis response in females. *Adnp* expression was correlated in a sex-dependent manner with CatWalk gait measurements [10] (front paws, males only and hind left paw, males and females). As expected from the pattern of gene expression, *Myl2* correlated with CatWalk gait measurements in females only in both hind paws.

3.5. ADNP is Functionally Associated with Multiple Muscle Disease Proteins

Given the tight association of ADNP expression levels with key motor dysfunctions, we asked if the mutated proteins causing these diseases (Table S1) are linked with ADNP at the protein level. STRING analysis for functional interactions included the mutated muscle disease-causing proteins (Figure 6B) alpha-actin (ACTA1), a major cytoskeletal gene, MAP1LC3B, a protein regulating autophagy, directly binding ADNP [13,27] and for ALS, C9orf72, a gene also linked to autophagy [68] and interacting with CNBP (causing DM2). In this respect, CNBP interacts with the α subunit of the dystroglycan complex, a core component of the multimeric dystrophin-glycoprotein complex, which regulates membrane stability [69]. As predicted, our results identified a tight network of proteins associated with cytoskeleton and muscle function (Figure 6B). Importantly, muscle *Myl2*, discovered here as not only regulated by ADNP in a sex-dependent manner but also corrected by NAP treatment, was seen as an integral part of the protein network regulating muscle function. Indeed, MYL2 has an obvious association with myosin’s essential role in muscle contraction.

3.6. Choosing the Most Efficient Guide RNA for Muscle *Adnp* Knockdown

To provide direct evidence for the involvement of *Adnp* in adult muscle function, we virally-delivered the CRISPR-mediated knockdown of *Adnp* to the gastrocnemius muscle of

Cas9 adult mice. Specifically, we designed three sgRNAs (G60, G67, and G68) to target the second coding exon (exon No.4) of the mouse *Adnp* gene (Figure 7A). To quantitatively determine the relative efficiency of the designed sgRNAs, we transfected these sgRNAs and the Cas9 protein into NIH 3T3 cells (of murine origin), and after two weeks evaluated the Adnp protein levels (Figure 7B and Figure S5). All three sgRNAs showed a significant reduction in Adnp protein levels, with G68 showing the most profound knockdown (98.65% reduction) compared with the appropriate control (Figure 7B). The off-target effect of G68 (listed in Table S3) has been proven to be most likely negligible. Thus, lentiviruses with sgRNA G68 and a stuffer (a stretch of poly T causing premature termination of RNA pol III as a control [70]) were prepared as described before [58] and injected into gastrocnemius muscles of 3-month-old Cas9-expressing mice. One-month post-injection, during which animals were treated with intranasal NAP or vehicle (DD, Methods), we performed motor behavioral experiments including the treadmill test and the CatWalk gait analyses.

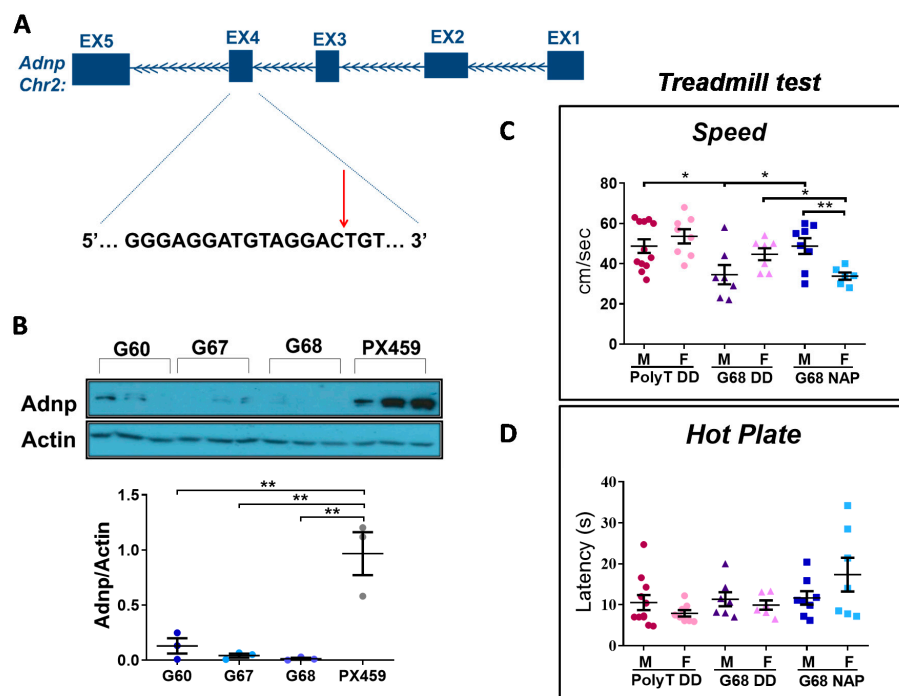


Figure 7. CRISPR/Cas9-mediated knockdown to the *Adnp* gene. (A) A schematic representation of the targeted second coding exon (exon No.4) of the mouse *Adnp* gene sequence. The 18-nucleotide sgRNA target sequence is depicted in black, and the red arrowhead indicates the Cas9 cleavage site. (B) A successful knockdown of *Adnp* in culture by the CRISPR-Cas9 technology: NIH 3T3 cells were transfected with PX459 plasmid, encoding 3 different *Adnp* sgRNA (termed 60, 67, 68), and an empty plasmid as control (termed PX459), the protein was extracted and subjected to Western blotting (staining with an ADNP antibody and normalized to Actin). One-way ANOVA followed by a Tukey post hoc test revealed that all sgRNA induce a significant knockdown ($n = 3$, $* p = 0.002$, $** p = 0.001$, $** p = 0.001$ for 60, 67, 68 respectively). sgRNA 68 showed the most profound knockdown with a 98.65% reduction in ADNP protein levels, compared with control. All sgRNAs targeted the second coding exon (exon No.4) of ADNP. sgRNA sequences were as follows: 68: 5'-GGGAGGATGTAGGACTGT-3', 67: 5'-CAGTCCTACATCCTCCCATG-3', 60: 5'-AACACTACATGGGAGGATGT-3'. (C) Treadmill test: A significant reduction in maximum running speed was observed in the G68 male mice group compared to Poly T DD ($* p < 0.05$) and NAP-treated G68 mice ($* p < 0.05$). Poly T (males $n = 12$; females $n = 8$), G68 DD (males $n = 7$; females $n = 7$) and G68 NAP groups (males $n = 8$; females $n = 7$). Furthermore, sex differences were found in the G68 NAP-treated group ($** p < 0.01$). (D) No significant differences were observed in the hot plate test. Analysis was performed by using an unpaired Student's *t*-test. Poly T (males $n = 12$; females $n = 8$), G68 DD (males $n = 7$; females $n = 7$) and G68 NAP groups (males $n = 8$; females $n = 7$).

3.7. Adult *Adnp* Knockdown Male Mice Exhibit Aberrant Motor Performance in The Treadmill Test

In the treadmill test (Figure 7C), we assessed: total distance run, time until exhaustion, and maximum speed. The maximum running speed was significantly lower in G68 DD male mice, compared with Poly T DD, and G68 NAP treatment ameliorated this deficit (Figure 7C). Furthermore, sex differences were found in the G68 NAP-treated group (Figure 7C and Figure S6), with the female group showing reduced performance in all tested parameters, compared with male mice. Additionally, G68 DD male mice remained on the treadmill for significantly shorter periods of time compared with the Poly T DD group (Figure S6A), conclusively running shorter distances (Figure S6B). NAP-treated G68 male mice exhibited a trend of improvement ($p = 0.053$) in time until exhaustion, as well as in running performance ($p = 0.06$) (Figure S6A and S6B, respectively). Importantly, we also performed a hot plate test to exclude the possibility that the phenotype observed in the G68 mice was a consequence of sensory deficits caused by the lentiviral injection procedure. We did not observe any significant changes between the tested groups (Figure 7D).

3.8. Impaired Gait Parameters in *Cas9* Female Mice *Adnp* Knockdown Are Ameliorated by NAP Treatment

Using the Catwalk apparatus, we estimated a substantial number of gait parameters divided into several categories: run characterization, interlimb coordination (swing speed, body speed, step cycle, and base of support (BOS)), as well as temporal and spatial parameters. (Our previous paper [10] details the precise measurement characteristics).

Figure 8 depicts an extensive analysis of gait parameters that were affected by *Adnp* knockdown and corrected by NAP treatment. Interestingly, those changes were discovered in females, whereas males were mostly unaffected.

Specifically, results showed that swing speed was significantly decreased in G68 DD female mice, as compared with the Poly T DD group and this decrease was ameliorated by NAP treatment (Figure 8A). Correspondingly, body speed displayed a similar pattern (Figure 8B). Our analysis also revealed a significant increase in the duration of the step cycle in G68 DD female mice, as compared with Poly T DD and NAP-treated G68 groups (Figure 8C).

Another coordination-related parameter analyzed was the BOS. Here, we observed a significant decrease in BOS (hind paws) in the G68 DD female group in relation to the Poly T DD and the NAP-treated G68 mice (Figure 8D).

A significant difference between Poly T DD and G68 DD mice was also found in temporal parameters. Single stance, was significantly higher in the RH G68 DD females, compared with Poly T DD and NAP-treated (ameliorated) G68 DD mice. This was the only parameter ameliorated by NAP treatment, which showed an increase because of *Adnp* knockdown and an effect on the right hind paw (Figure 8E).

The spatial parameters were also altered in G68 DD female mice (Figure 8F). G68 DD female mice showed a significantly reduced LF paw contact pressure with the walkway, compared with the Poly T DD group, measured as the mean intensity of the 15 most intense pixels and corrected by NAP treatment (Figure 8F). Sex differences were also observed in the G68 DD group (** $p < 0.01$). An additional summary of significant changes of the affected parameters by either the *Adnp* genotype, or the NAP treatment or by sex in CatWalk gait results is presented in Table S4, showing multiple small, but significant differences.

To exclude the possibility that the observed phenotype in G68 mice was attributed to the injection procedure, we used an additional mouse group injected only with the carrier Neurobasal (NB) medium. Figure S7 shows no significant differences between the Poly T DD and NB groups, strengthening the above results.

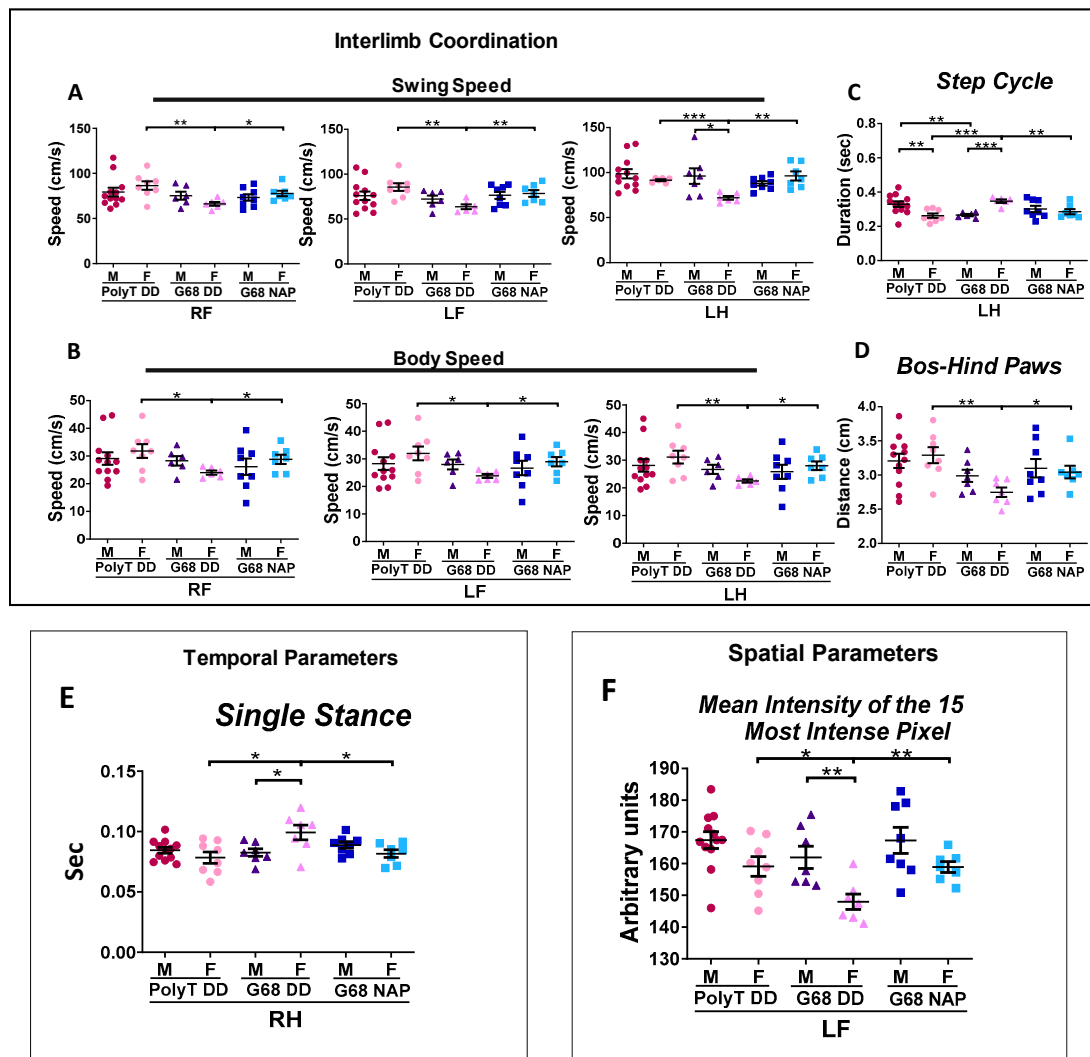


Figure 8. G68 female mice aberrant CatWalk behavior is ameliorated by NAP. CatWalk gait analysis: Poly T (males $n = 12$; females $n = 8$), G68 DD (males $n = 7$; females $n = 7$) and G68 NAP groups (males $n = 8$; females $n = 7$). (A) Swing Speed was significantly decreased in G68 female mice, compared with the Poly T DD group, and corrected by NAP treatment: RF (** $p < 0.01$, * $p < 0.05$, respectively); LF (** $p < 0.01$, ** $p < 0.01$, respectively); LH (** $p < 0.01$, ** $p < 0.01$, respectively). Additionally, sex effect was observed in G68 DD group (* $p < 0.05$). (B) Body Speed was significantly decreased in G68 female mice, compared with the Poly T DD group, and corrected by NAP treatment: RF (* $p < 0.05$, * $p < 0.05$, respectively); LF (* $p < 0.05$, * $p < 0.05$, respectively); LH (** $p < 0.01$, * $p < 0.05$, respectively). (C) Step cycle an inverse impact was observed in males and females. In G68 DD males, the duration of the step cycle was significantly shorter (** $p < 0.01$), compared with the Poly T DD male group, whereas G68 DD females displayed a significantly longer step cycle, compared with the Poly T DD female group (** $p < 0.01$), normalized by NAP treatment (** $p < 0.01$). Also, sex differences were found in Poly T DD (** $p < 0.01$) and G68 DD groups (** $p < 0.01$). (D) Base of support (BOS) was significantly smaller in G68 DD female mice, compared with Poly T DD female mice (** $p < 0.01$) and NAP-treated G68 female mice (* $p < 0.05$). (E) Single stance was significantly longer in G68 DD female mice, compared with the Poly T DD (* $p < 0.05$) and NAP-treated G68 female mice (* $p < 0.05$). Additionally, sex differences were observed in the G68 DD group (* $p < 0.05$). (F) The Mean Intensity of the 15 Most Intense Pixel was significantly decreased in the G68 DD, compared with the Poly T DD female mice (* $p < 0.05$), and NAP-treated G68 female mice (** $p < 0.01$). Sex differences were observed in the G68 DD group (** $p < 0.01$).

4. Discussion

Our paper investigated the involvement of *Adnp* expression and NAP ameliorative effects in developing/adult muscle function at four levels: (A) the single cell, (B) human muscle diseases, (C) inborn *Adnp* deficiency (*Adnp*^{+/-} mice), and (D) adult muscle genome editing, *Adnp* knockdown. Together, *ADNP/Adnp* was identified in the single developing/aging muscle cell. *ADNP* expression presented predictive values to human muscle diseases. The mechanistic mouse results implicated *Adnp* regulation of microtubules and myosin (*Myl2*) as key players regulating behavioral outcomes in a sex/age-dependent manner. Importantly, direct *Adnp* local knockdown exerted sex-specific muscle defects, which were partially ameliorated by intranasal NAP treatment.

Given our results correlating between *ADNP* expression and human muscle aging and our current transcriptomic analyses at the single human muscle cell level indicating a potentially crucial role for *ADNP* in muscle development, as exemplified in the *ADNP* syndrome [5,7,8,71], we investigated the involvement of *ADNP* in several NMJ pathologies (some highly prevalent in males) and discovered significant dysregulation. A Comparison of *ADNP* levels in Pompe [41], DMD [42], DM2 [43], and TMD [43] muscles with healthy controls revealed highly significant (essentially nonintersecting) downregulation compared with control values. DMD presented an exception with some overlap between disease and control individuals, regardless, also in the DMD case, *ADNP* levels were predictive of the disease. In this respect, Pompe and TMD are linked with autophagy (Table S1), which is in turn linked with *ADNP* [26,27]. DM2 is associated with aberrant RNA splicing, also linked with *ADNP* function [20,72]. DMD (dystrophin absence) is linked to the cytoskeleton, with dystrophin binding to actin [73] and actin filaments interacting with microtubules [74,75].

In BMD (dystrophin mutation), dysferlin mutation (*DYSF*, associated with mitochondrial function) [63], fukutin-related protein mutation (*FKRP*, associated with extracellular matrix) [64] and ALS (Table S1), *ADNP* transcript levels, although predictive of the pathology, not showing complete separation, increased compared with matched healthy controls. These increases may represent an age/sex/muscle-dependent compensatory effect, also resulting from *ADNP* auto-regulation of its own gene expression [9,76]. Regardless, in a zebrafish model of *FKRP* mutation, *NAD*⁺ supplementation prior to muscle development improved muscle structure, myotendinous junction structure, and muscle function [64], with *ADNP* highly correlated with *NMNAT1* (e.g., the aging human muscle [13]). Furthermore, in the *SOD1-G93A* mouse model of ALS, we have shown an involvement of microtubule-tau pathology and protection by NAP [77] (Table S1). These results also connect with the extensive interactions of cellular cytoskeletal elements affecting microtubule dynamics [78], with *ADNP/NAP* playing an essential role in maintaining microtubule dynamicity and regulating multiple gene expression patterns, in a sex-dependent manner [25]. Importantly, our functional analysis of muscle disease protein interactions (Figure 6) tightly linked *ADNP* with human muscle contraction and implicated direct *ADNP* interactions with muscle motor disease inflicting proteins. These interactions are intimately interwoven with our findings of decreased microtubules in the limb muscle of the *Adnp*^{+/-} mice, which was exacerbated by aging. We suggest that deficits in the *ADNP*/microtubule cytoskeletal network may increase the susceptibility of the NMJ to physical disruption. Such alterations in the microtubule network density would have a profound impact on the contractility of the *Adnp*^{+/-} muscle. Thus, our results imply an important role for *ADNP* in maintaining proper NMJ structure and function and as emphasized above, with STRING pathway analysis strongly linking *ADNP* with key muscle disease proteins, at the level of cytoskeletal protein organization.

To further understand the differential involvement of *ADNP* in the various muscle disorders, we have also assessed the levels of the *ADNP* binding proteins EB1 (*MAPRE1*) and EB3 (*MAPRE3*). Our results indicated that in all the diseases showing *ADNP* decreases, *MAPRE1* increased, and Pompe disease even showed an additional increase in *MAPRE3*, potentially compensating for the apparent *ADNP* deficiency. In contrast, the increase of *ADNP* in BMD and ALS was coupled to an increase in *MAPRE1*, while *DYSF*- and *FKRP*-related diseases did not show a significant change in *MAPRE1*. These results suggested differential regulation of *ADNP/MAPRE1* in the different muscle

diseases, with *MAPRE1* consistently increasing (or showing no significant change) and with *ADNP* auto-regulating its own transcript levels [9,76] in a feedback mechanism. Regardless, as indicated above, in an ALS mouse model, NAP provided protection [77]. Furthermore, attesting to the importance of the *MAPRE1,3* function in muscle diseases is the direct link for *MAPRE3* to distal hereditary motor neuropathy type 7 [79].

It should be mentioned that *ADNP* plays a dual role, one cytoplasmic with strong microtubule-autophagy-linked activities [13,15,23,26,27,80] and one as a transcription factor, chromatin remodeler [9,16,17]. Our previous gene array and RNA-seq results did not emphasize the *ADNP* regulation of the muscle disease genes studied here [9,25,80]. Indeed, some regulation may occur, with *ADNP* interacting with CCCTC-binding factor (CTCF) sites [19], enriched in many genes [81]. However, the low correlations observed at the transcriptomic level (Figure 3) contrasted with the strong data regarding cytoskeletal interactions, imply altered cytoskeletal/autophagy functions as a consequence of muscle gene mutation. Together, these protein interactions may affect *ADNP* transcript cytoplasmic/nuclear content, with *ADNP* regulating its own transcript [9,76], predictive of motor disease.

Interestingly, cytoskeletal reorganization plays an important role in stretch-induced gene expression, further explaining the effects of *ADNP*/NAP on similar gene transcript expression, including the muscle-regulating *Myl2* gene [82].

Our current data suggest decreases in mouse male *Adnp* levels with aging in the gastrocnemius lower hind limb muscle/leg (Figure 4). Our previous data looking at the human vastus lateralis (higher hind limb muscle) suggested a modest increase in *ADNP* with aging as well as in the female biceps brachii (one of the main muscles of the upper arm) [13]. Importantly, in our current data (Figure 2) looking at diseases in which increases in *ADNP* were disease predictive, measurements were performed only in the vastus lateralis, correlating with our previous results in aging [13].

Additionally, the *ADNP* regulating peptide PACAP [12] was also shown to regulate muscle function in protection against outcome measures in a model of spinobulbar muscular atrophy [83]. Our most recent results also indicated *Adnp* regulation of the *Adcyap1r1* transcript, encoding the PACAP-specific, PAC1 receptor with a significant increase in bladder *Adcyap1r1* seen in *Adnp*^{+/-} versus *Adnp*^{+/+} females and correction of the female *Adnp*^{+/-} levels to the *Adnp*^{+/+} levels by NAP treatment [10]. These findings suggest a cross-regulation of *ADNP* and PACAP functions, with the PAC1 receptor antagonist, PACAP(6–38), reducing urinary bladder frequency and pelvic sensitivity in mice exposed to repeated variate stress [48] and with the majority of *ADNP* syndrome patients suffering from bladder training delay [5]. Furthermore, PACAP ameliorates *Adnp*^{+/-}-deficiencies that are exacerbated by stress [12].

Together, our results suggest that *ADNP* plays a key role in muscle, as previously shown for the brain. For example, our previous data showed a reduction in brain *ADNP* expression in aging animals, exhibiting microtubule-tau pathology (a mouse model for frontotemporal dementia) [84], and a positive correlation between *ADNP* serum concentrations and IQ test performance in elderly individuals [85]. Indeed, brain-muscle connections were also described before for the dystrophin gene [86], further extended to the autistic *ADNP* syndrome, with 96–100% of *ADNP* syndrome children suffering from motor impairments [5,8,87] and with motor impairments correlated with intellectual disability in *ADNP* cases [7]. Moreover, previous findings linked dysregulation of *ADNP* with aberrant synaptic function in neuropsychiatric diseases [88], possibly playing a part in NMJs, as shown here. Interestingly, sexual differences were found in *ADNP* expression in Alzheimer's disease (lymphocytes) [85] and in schizophrenia (post mortem brains and lymphocytes) [27,88].

Our single-cell analysis of the mouse data added an important dimension to the understanding of muscle diseases and *ADNP* potential involvement in these diseases, implicating additional tissues including, but not limited to adipose tissue stem cells, the pancreas, large intestine, and lung cells with potential multisystem effects.

However, correlation is not necessarily causation. To directly assess the effect of reduction in *Adnp* expression on motor functions we employed muscle *Adnp* knockdown in Cas9 expressing mice. Our outcome assessment included the automated CatWalk gait analysis, an exceedingly sensitive tool which allows the identification of an extensive number of gait and locomotion parameters with minimal human interference [89]. The CatWalk paradigm was previously implemented in the assessment of static and dynamic gait parameters in a variety of nerve injury models [90–92] including muscular dystrophies [90]. Our further results demonstrated, significant sex-dependent differences in CatWalk performance with G68 *Adnp*-knockdown female mice exhibiting abnormal interlimb coordination, temporal and spatial parameters. Interestingly, not all limbs were equally affected, suggesting a potential imbalance, which may be more emphasized in the female *Adnp*-knockdown mice.

Like the CatWalk, the treadmill system, assessing maximal endurance in mice, is usually implemented in models of neurodegenerative disorders including ALS [93], Huntington's disease [94,95] and Parkinson's disease [96,97] after therapeutic interventions [98,99], aiming at studying the potential roles of specific genes on muscle function [100,101]. This is a simple, sensitive, and objective test yielding high-throughput detection of endurance abnormalities [102]. *Adnp* knockdown G68 males were significantly impaired in treadmill performance, ameliorated by NAP treatment. Despite the abnormalities G68 DD knockdown female mice presented in the CatWalk test, these females were potentially able to significantly compensate treadmill performance defects in terms of speed, compared with G68 DD male mice. Furthermore, NAP treatment of G68 females resulted in reduced speed, potentially associated with the partial balancing of otherwise imbalanced paws, as observed in the CatWalk test (showing different effects for right, left, front and hind paws). Together, these results further emphasized sexual differences and established the G68 DD male mice as having significantly impaired treadmill behavior.

Regarding sexual dichotomy, we have shown here a very high correlation of *Adnp* expression to *Gnrhr*, tightly linked to sexual control. We have previously shown sex differences in ADNP expression in the mouse and the human hippocampus [21] as well as in the mouse hypothalamus [103]. Interestingly, not only in muscles, as seen here, but also in other tissues, *Adnp* regulates other genes in a sexually-dependent manner in the brain [21,25] as well in the spleen [28], which is also reflected in differential gut microbiota expression [104]. Importantly and pertinent to our results here, *Adnp* [25,28] and NAP [28] regulate the Y-chromosome gene lysine demethylase 5d (*Kdm5d*), which may be partially linked with cardiac muscle differentiation [105]. As ADNP was linked before to heart development in mice [46] and in humans [5], our current data may also imply sex-dependent ADNP effects in adult/aging heart diseases. Most interestingly, we have shown sexual dichotomy in microtubule dynamics also in association with *Adnp* expression [25], with ADNP regulating steroid pathways [80], impinging on sex differences in muscle function.

To summarize the discussion above, highlighting points for future investigations, we would like to point out the following interesting, but perhaps conflicting results.

(1) As indicated above, DMD and BMD are allelic disorders caused by the *DMD* (dystrophin) gene mutation. However, changes in the muscle expression level of ADNP were divided in opposite sides: downregulated in DMD (complete deletion of the X-linked *DMD* gene) and upregulated in BMD (*DMD* mutations). With the *DMD* protein [86] being one of the longest proteins known (3685 amino acid residues), *DMD* and BMD exhibit markedly different phenotypes (see also Table S1), including opposite regulation of ADNP as discovered here, which may be of interest for future investigations.

MAPRE1, encoding one of the cytoplasmic targets of ADNP [13], was increased in muscles of diseases with decreased muscle ADNP (Pompe, DM2, TMD, DMD, Figure 2). However, increases in muscle *MAPRE1* were also observed for BMD and ALS, diseases showing increases in ADNP (Figure 2), implicating additional players for further investigation. Similarly, while one may suggest that there is no difference in age and sex between TMD and ALS, these are two very different diseases, with TMD being a late-onset, autosomal dominant distal myopathy, resulting from mutations in the two last domains of titin (associated with the unfolded protein response and altered autophagy) and with ALS

being essentially a sporadic disease associated with several genetic deficits (Table S1). Here, *ADNP* and *MAPRE1* showed a negative correlation in TMD and a positive correlation (increases) in ALS, again suggesting additional mechanisms requiring further investigations.

(2) Our previous data showed that the expression level of human male *ADNP* increased with age in vastus lateralis and biceps brachii and similar age-dependent increases were observed in the male mouse gastrocnemius muscle up to 8 months of age [10]. Here, looking at 18- and 24-month-old mice compared to 3-month-old mice, at the single-cell level, a decrease in the very old age in the male mouse muscle limbs was observed (Figure 4). These results imply that at a very old age, *ADNP* may also decrease in the human muscle.

(3) In the results of the *Adnp*^{+/-} mice (Figures 5 and 6), there was an age-dependent difference in terms of genotype related muscle *Adnp* expression, significantly reducing in the 7-month-old male (but not female) mice, with *Myl2* correlating with the hanging wire behavior only in females. In contrast, in 19–27-day-old mice, muscle *Adnp* was significantly decreased in both *Adnp*^{+/-} males and females, regardless, *Myl2* was again only decreased in *Adnp*^{+/-} females and corrected by NAP treatment. At this young muscle age, *Adnp*^{+/+} control males expressed higher *Adnp* and lower *Myl2* concentrations than females, suggesting age and sex-dependent regulation as was noted before in the brain and the spleen of these mice [25,28].

(4) Similar to the *Adnp*^{+/-} mice, behavioral outcomes of the genetically edited mice were affected differently by gender (Figures 7 and 8). Abnormalities were found in the treadmill test in males and in the CatWalk test in females. While treadmill performance was improved by NAP treatment in males, it decreased in females in the genome-edited mice. However, in the CatWalk test, NAP significantly improved the *Adnp* knock-down mouse behavior.

Together with the critical points above, our study limitations include the inability to look at all human different muscles in health and all muscle diseases, to identify a precise pattern and specificity. The strength of our findings resides in the emphasis of *ADNP*'s crucial role in muscle function, coupled to its binding partners *MAPRE1* (EB1) and *MAPRE3* (EB3) and the clinical significance of amelioration by NAP (CP201, davunetide) treatment, with marked sexual dichotomy. In this respect, davunetide was tested before in progressive supranuclear palsy (PSP) affecting muscle function and while presenting a clean toxicology profile, it did not present efficacy [106]. However, in this previous PSP clinical study, a pure 4 repeat tauopathy, which may not entirely fit the NAP mechanism of action [24], males and females were mixed and not analyzed separately, which may have further skewed the results. Given our discovered predictive value of *ADNP* levels on muscle function and NAP ameliorative effects in the preclinical setting, future clinical trials should take advantage of individualized precision, personalized medicine with CP201 (davunetide), and pipeline products [25], as well as *ADNP* regulating neuropeptides [83], presenting potential adjuvant therapeutics.

Supplementary Materials: The following are available online at <http://www.mdpi.com/2073-4409/9/10/2320/s1>, Table S1: Selected muscle diseases, Table S2: A tabular summary of the different patients and aged matched controls characterizations, Table S3: G68 off targets. The vast majority have 4 mismatches with the G68 sequence, some have 3 and only 1-off target has 2 mismatches (intronic), making the effects of these targets mostly negligible, Table S4. Summary of significant fold-changes in reference to the tested parameters in CatWalk gait analysis affected by *Adnp* knockdown, NAP treatment and sex, Figure S1. Single human muscle cell *ADNP* cellular distribution at different time points during gestation, Figure S2 Single cell specific gene transcriptomes of hind limbs from human fetuses of 9 weeks, Figure S3. Overall systemic loss of correlation of expression of *Adnp* and disease genes at the single cell level, Figure S4. Representative whole-mount NMJ immunostaining of 14-month-old (*Adnp*^{+/+} CB *n* = 4; *Adnp*^{+/-} CB *n* = 2) male mice, Figure S5. A successful knockdown of *Adnp* in culture by the CRISPR-Cas9 technology: Full Western blot control for Figure 7B, Figure S6. G68 male mice displayed a significantly reduced max ability to run on treadmill compared with the Poly T DD group, Figure S7. No significant differences were found between the Poly T DD and the neurobasal (NB) medium injected groups.

Author Contributions: O.K. provided input in the establishment of the research hypothesis, project design, performed experiments, and provided an impact on data analysis and article writing. G.K. designed sgRNA and evaluated its efficacy. S.S. supplied important input into project design, provided tissues from *Adnp*^{+/-} mice, and contributed to CatWalk gait analysis performance. A.H. provided all the human single-cell analysis and data. M.S. helped in lentiviral production. L.B. supported and provided input in all mouse behavioral

analysis. I.J. performed extensive statistical analyses. E.G. supported animal daily treatment, mouse sacrifice, and tissue excision. R.P. and T.I. provided all the single mouse data and contributed to the bioinformatics analysis. I.G. designed, led, and orchestrated the entire project, provided funding, designed experiments, analyzed the data, prepared graphs, and wrote the article. All authors have read and agreed to the published version of the manuscript.

Funding: This work was partially supported by the following grants (IG): European Research Area Network (ERA-NET) Neuron ADNPinMED, the US–Israel Binational Science Foundation—US National Science Foundation (BSF-NSF 2016746), the Alberto Moscona Nisim (AMN) Foundation for the Advancement of Science, Art and Culture in Israel, as well as by Drs. Ronith and Armand Stemmer and Arthur Gerbi (French Friends of Tel Aviv University) and Anne and Alex Cohen (Canadian Friends of Tel Aviv University). O.K. is and S.S. was supported by the Israeli BioInnovators Fellowship and Mentors by Teva. S.S. is a former Levi Eshkol fellow supported by the Israel Ministry of Science and Technology, and a former awardee of the Tel Aviv University GRTF and The Naomi Foundation, as well as The Eldee Foundation/Bloomfield Family of Montreal awards for student exchange (Tel Aviv University/McGill University). This work is in partial fulfillment of O.K. and G.K. Ph.D. thesis requirements at the Dr. Miriam and Sheldon G. Adelson Graduate School of Medicine, Sackler Faculty of Medicine, Tel Aviv University.

Acknowledgments: We thank Uri Ashery and Yoav Benjamini, Ph.D. mentors of M.S. and I.J., respectively for excellent collaborations. Dan Peer from Tel-Aviv University for generously providing us Cas9 mice. We also thank Gal Hacoheh-Kleiman for the help with *Adnp*^{+/-} mouse colony and to Colin J. Barnstable for generously collaborating and providing the TUB2.1 antibody. Gratitude also goes to Noy Amram, Irena Voinsky, Shahar Laks, Adi Linevitz Ovsiovich, and Adi Zaslavsky for technical and editorial valuable help.

Conflicts of Interest: Professor Illana Gozes is the Chief Scientific Officer of Coronis Neurosciences. NAP (CP201) use is under patent protection (US patent nos. US7960334, US8618043, and USWO2017130190A1).

References

1. Gozes, I.; Bassan, M.; Zamostiano, R.; Pinhasov, A.; Davidson, A.; Giladi, E.; Perl, O.; Glazner, G.W.; Brenneman, D.E. A novel signaling molecule for neuropeptide action: Activity-dependent neuroprotective protein. *Ann. N. Y. Acad. Sci.* **1999**, *897*, 125–135. [[CrossRef](#)]
2. Zamostiano, R.; Pinhasov, A.; Gelber, E.; Steingart, R.A.; Seroussi, E.; Giladi, E.; Bassan, M.; Wollman, Y.; Eyre, H.J.; Mulley, J.C.; et al. Cloning and characterization of the human activity-dependent neuroprotective protein. *J. Biol. Chem.* **2001**, *276*, 708–714. [[CrossRef](#)]
3. Bassan, M.; Zamostiano, R.; Davidson, A.; Pinhasov, A.; Giladi, E.; Perl, O.; Bassan, H.; Blat, C.; Gibney, G.; Glazner, G.; et al. Complete sequence of a novel protein containing a femtomolar-activity-dependent neuroprotective peptide. *J. Neurochem.* **1999**, *72*, 1283–1293. [[CrossRef](#)] [[PubMed](#)]
4. Pinhasov, A.; Mandel, S.; Torchinsky, A.; Giladi, E.; Pittel, Z.; Goldsweig, A.M.; Servoss, S.J.; Brenneman, D.E.; Gozes, I. Activity-dependent neuroprotective protein: A novel gene essential for brain formation. *Brain Res. Dev. Brain Res.* **2003**, *144*, 83–90. [[CrossRef](#)]
5. Van Dijck, A.; Vulto-van Silfhout, A.T.; Cappuyns, E.; van der Werf, I.M.; Mancini, G.M.; Tzschach, A.; Bernier, R.; Gozes, I.; Eichler, E.E.; Romano, C.; et al. Clinical Presentation of a Complex Neurodevelopmental Disorder Caused by Mutations in ADNP. *Biol. Psychiatry* **2019**, *85*, 287–297. [[CrossRef](#)] [[PubMed](#)]
6. Levine, J.; Cohen, D.; Herman, C.; Verloes, A.; Guinchat, V.; Diaz, L.; Cravero, C.; Mandel, A.; Gozes, I. Developmental Phenotype of the Rare Case of DJ Caused by a Unique ADNP Gene De Novo Mutation. *J. Mol. Neurosci. MN* **2019**, *68*, 321–330. [[CrossRef](#)] [[PubMed](#)]
7. Arnett, A.B.; Rhoads, C.L.; Hoekzema, K.; Turner, T.N.; Gerdts, J.; Wallace, A.S.; Bedrosian-Sermone, S.; Eichler, E.E.; Bernier, R.A. The autism spectrum phenotype in ADNP syndrome. *Autism Res. Off. J. Int. Soc. Autism Res.* **2018**, *11*, 1300–1310. [[CrossRef](#)] [[PubMed](#)]
8. Gozes, I.; Van Dijck, A.; Hacoheh-Kleiman, G.; Grigg, I.; Karmon, G.; Giladi, E.; Eger, M.; Gabet, Y.; Pasmanik-Chor, M.; Cappuyns, E.; et al. Premature primary tooth eruption in cognitive/motor-delayed ADNP-mutated children. *Transl. Psychiatry* **2017**, *7*, e1043. [[CrossRef](#)] [[PubMed](#)]
9. Mandel, S.; Rechavi, G.; Gozes, I. Activity-dependent neuroprotective protein (ADNP) differentially interacts with chromatin to regulate genes essential for embryogenesis. *Dev. Biol.* **2007**, *303*, 814–824. [[CrossRef](#)] [[PubMed](#)]
10. Kapitansky, O.; Sragovich, S.; Jaljuli, I.; Hadar, A.; Giladi, E.; Gozes, I. Age and Sex-Dependent ADNP Regulation of Muscle Gene Expression Is Correlated with Motor Behavior: Possible Feedback Mechanism with PACAP. *Int. J. Mol. Sci.* **2020**, *21*, 6715. [[CrossRef](#)] [[PubMed](#)]

11. Girard, B.M.; Campbell, S.E.; Beca, K.I.; Perkins, M.; Hsiang, H.; May, V.; Vizzard, M.A. Intrabladder PAC1 Receptor Antagonist, PACAP(6-38), Reduces Urinary Bladder Frequency and Pelvic Sensitivity in Mice Exposed to Repeated Variate Stress (RVS). *J. Mol. Neurosci. MN* **2020**. [[CrossRef](#)]
12. Sragovich, S.; Ziv, Y.; Vaisvaser, S.; Shomron, N.; Hendler, T.; Gozes, I. The autism-mutated ADNP plays a key role in stress response. *Transl. Psychiatry* **2019**, *9*, 235. [[CrossRef](#)] [[PubMed](#)]
13. Ivashko-Pachima, Y.; Hadar, A.; Grigg, I.; Korenkova, V.; Kapitansky, O.; Karmon, G.; Gershovits, M.; Sayas, C.L.; Kooy, R.F.; Attems, J.; et al. Discovery of autism/intellectual disability somatic mutations in Alzheimer's brains: Mutated ADNP cytoskeletal impairments and repair as a case study. *Mol. Psychiatry* **2019**. [[CrossRef](#)] [[PubMed](#)]
14. de Guia, R.M.; Agerholm, M.; Nielsen, T.S.; Consitt, L.A.; Sogaard, D.; Helge, J.W.; Larsen, S.; Brandauer, J.; Houmard, J.A.; Treebak, J.T. Aerobic and resistance exercise training reverses age-dependent decline in NAD(+) salvage capacity in human skeletal muscle. *Physiol. Rep.* **2019**, *7*, e14139. [[CrossRef](#)] [[PubMed](#)]
15. Ivashko-Pachima, Y.; Sayas, C.L.; Malishkevich, A.; Gozes, I. ADNP/NAP dramatically increase microtubule end-binding protein-Tau interaction: A novel avenue for protection against tauopathy. *Mol. Psychiatry* **2017**, *22*, 1335–1344. [[CrossRef](#)] [[PubMed](#)]
16. Mandel, S.; Spivak-Pohis, I.; Gozes, I. ADNP differential nucleus/cytoplasm localization in neurons suggests multiple roles in neuronal differentiation and maintenance. *J. Mol. Neurosci. MN* **2008**, *35*, 127–141. [[CrossRef](#)] [[PubMed](#)]
17. Mandel, S.; Gozes, I. Activity-dependent neuroprotective protein constitutes a novel element in the SWI/SNF chromatin remodeling complex. *J. Biol. Chem.* **2007**, *282*, 34448–34456. [[CrossRef](#)]
18. Ferrari, R.; de Llobet Cucalon, L.I.; Di Vona, C.; Le Dilly, F.; Vidal, E.; Lioutas, A.; Oliete, J.Q.; Jochem, L.; Cutts, E.; Dieci, G.; et al. TFIIC Binding to Alu Elements Controls Gene Expression via Chromatin Looping and Histone Acetylation. *Mol. Cell* **2020**, *77*, 475–487.e11. [[CrossRef](#)]
19. Kaaij, L.J.T.; Mohn, F.; van der Weide, R.H.; de Wit, E.; Buhler, M. The ChAHP Complex Counteracts Chromatin Looping at CTCF Sites that Emerged from SINE Expansions in Mouse. *Cell* **2019**, *178*, 1437–1451.e14. [[CrossRef](#)]
20. Schirer, Y.; Malishkevich, A.; Ophir, Y.; Lewis, J.; Giladi, E.; Gozes, I. Novel marker for the onset of frontotemporal dementia: Early increase in activity-dependent neuroprotective protein (ADNP) in the face of Tau mutation. *PLoS ONE* **2014**, *9*, e87383. [[CrossRef](#)]
21. Malishkevich, A.; Amram, N.; Hacoheh-Kleiman, G.; Magen, I.; Giladi, E.; Gozes, I. Activity-dependent neuroprotective protein (ADNP) exhibits striking sexual dichotomy impacting on autistic and Alzheimer's pathologies. *Transl. Psychiatry* **2015**, *5*, e501. [[CrossRef](#)] [[PubMed](#)]
22. Gkogkas, C.G.; Khoutorsky, A.; Ran, I.; Rampakakis, E.; Nevarko, T.; Weatherill, D.B.; Vasuta, C.; Yee, S.; Truitt, M.; Dallaire, P.; et al. Autism-related deficits via dysregulated eIF4E-dependent translational control. *Nature* **2013**, *493*, 371–377. [[CrossRef](#)]
23. Oz, S.; Kapitansky, O.; Ivashco-Pachima, Y.; Malishkevich, A.; Giladi, E.; Skalka, N.; Rosin-Arbesfeld, R.; Mittelman, L.; Segev, O.; Hirsch, J.A.; et al. The NAP motif of activity-dependent neuroprotective protein (ADNP) regulates dendritic spines through microtubule end binding proteins. *Mol. Psychiatry* **2014**, *19*, 1115–1124. [[CrossRef](#)] [[PubMed](#)]
24. Ivashko-Pachima, Y.; Maor-Nof, M.; Gozes, I. NAP (davunetide) preferential interaction with dynamic 3-repeat Tau explains differential protection in selected tauopathies. *PLoS ONE* **2019**, *14*, e0213666. [[CrossRef](#)]
25. Amram, N.; Hacoheh-Kleiman, G.; Sragovich, S.; Malishkevich, A.; Katz, J.; Touloumi, O.; Lagoudaki, R.; Grigoriadis, N.C.; Giladi, E.; Yeheskel, A.; et al. Sexual divergence in microtubule function: The novel intranasal microtubule targeting SKIP normalizes axonal transport and enhances memory. *Mol. Psychiatry* **2016**, *21*, 1467–1476. [[CrossRef](#)] [[PubMed](#)]
26. Esteves, A.R.; Gozes, I.; Cardoso, S.M. The rescue of microtubule-dependent traffic recovers mitochondrial function in Parkinson's disease. *Biochim. Biophys. Acta* **2014**, *1842*, 7–21. [[CrossRef](#)]
27. Merenlender-Wagner, A.; Malishkevich, A.; Shemer, Z.; Udawela, M.; Gibbons, A.; Scarr, E.; Dean, B.; Levine, J.; Agam, G.; Gozes, I. Autophagy has a key role in the pathophysiology of schizophrenia. *Mol. Psychiatry* **2015**, *20*, 126–132. [[CrossRef](#)]
28. Hacoheh-Kleiman, G.; Sragovich, S.; Karmon, G.; Gao, A.Y.L.; Grigg, I.; Pasmanik-Chor, M.; Le, A.; Korenkova, V.; McKinney, R.A.; Gozes, I. Activity-dependent neuroprotective protein deficiency models synaptic and developmental phenotypes of autism-like syndrome. *J. Clin. Investig.* **2018**, *128*, 4956–4969. [[CrossRef](#)]

29. Meola, G.; Cardani, R. Myotonic dystrophy type 2 and modifier genes: An update on clinical and pathomolecular aspects. *Neurol. Sci. Off. J. Ital. Neurol. Soc. Ital. Soc. Clin. Neurophysiol.* **2017**, *38*, 535–546. [[CrossRef](#)]
30. Yiu, E.M.; Kornberg, A.J. Duchenne muscular dystrophy. *J. Paediatr. Child Health* **2015**, *51*, 759–764. [[CrossRef](#)]
31. Belanto, J.J.; Mader, T.L.; Eckhoff, M.D.; Strandjord, D.M.; Banks, G.B.; Gardner, M.K.; Lowe, D.A.; Ervasti, J.M. Microtubule binding distinguishes dystrophin from utrophin. *Proc. Natl. Acad. Sci. USA* **2014**, *111*, 5723–5728. [[CrossRef](#)] [[PubMed](#)]
32. Capitano, D.; Moriggi, M.; Torretta, E.; Barbacini, P.; De Palma, S.; Vigano, A.; Lochmuller, H.; Muntoni, F.; Ferlini, A.; Mora, M.; et al. Comparative proteomic analyses of Duchenne muscular dystrophy and Becker muscular dystrophy muscles: Changes contributing to preserve muscle function in Becker muscular dystrophy patients. *J. Cachexiasarcopenia Muscle* **2020**, *11*, 547–563. [[CrossRef](#)] [[PubMed](#)]
33. Andrews, J.G.; Wahl, R.A. Duchenne and Becker muscular dystrophy in adolescents: Current perspectives. *Adolesc. Healthmed. Ther.* **2018**, *9*, 53–63. [[CrossRef](#)] [[PubMed](#)]
34. Kohler, L.; Puertollano, R.; Raben, N. Pompe Disease: From Basic Science to Therapy. *Neurother. J. Am. Soc. Exp. Neurother.* **2018**, *15*, 928–942. [[CrossRef](#)]
35. Savarese, M.; Sarparanta, J.; Vihola, A.; Udd, B.; Hackman, P. Increasing Role of Titin Mutations in Neuromuscular Disorders. *J. Neuromuscul. Dis.* **2016**, *3*, 293–308. [[CrossRef](#)]
36. Bansal, D.; Miyake, K.; Vogel, S.S.; Groh, S.; Chen, C.C.; Williamson, R.; McNeil, P.L.; Campbell, K.P. Defective membrane repair in dysferlin-deficient muscular dystrophy. *Nature* **2003**, *423*, 168–172. [[CrossRef](#)] [[PubMed](#)]
37. Gerin, I.; Ury, B.; Breloy, I.; Bouchet-Seraphin, C.; Bolsee, J.; Halbout, M.; Graff, J.; Vertommen, D.; Muccioli, G.G.; Seta, N.; et al. ISPD produces CDP-ribitol used by FKTN and FKRP to transfer ribitol phosphate onto alpha-dystroglycan. *Nat. Commun.* **2016**, *7*, 11534. [[CrossRef](#)]
38. Masrori, P.; Van Damme, P. Amyotrophic lateral sclerosis: A clinical review. *Eur. J. Neurol.* **2020**. [[CrossRef](#)]
39. Xi, H.; Langerman, J.; Sabri, S.; Chien, P.; Young, C.S.; Younesi, S.; Hicks, M.; Gonzalez, K.; Fujiwara, W.; Marzi, J.; et al. A Human Skeletal Muscle Atlas Identifies the Trajectories of Stem and Progenitor Cells across Development and from Human Pluripotent Stem Cells. *Cell Stem Cell* **2020**, *27*, 181–185. [[CrossRef](#)]
40. USCS Cell Browser. Available online: <https://skeletal-muscle.cells.ucsc.edu> (accessed on 15 August 2020).
41. Palermo, A.T.; Palmer, R.E.; So, K.S.; Oba-Shinjo, S.M.; Zhang, M.; Richards, B.; Madhiwalla, S.T.; Finn, P.F.; Hasegawa, A.; Ciociola, K.M.; et al. Transcriptional response to GAA deficiency (Pompe disease) in infantile-onset patients. *Mol. Genet. Metab.* **2012**, *106*, 287–300. [[CrossRef](#)]
42. Haslett, J.N.; Sanoudou, D.; Kho, A.T.; Han, M.; Bennett, R.R.; Kohane, I.S.; Beggs, A.H.; Kunkel, L.M. Gene expression profiling of Duchenne muscular dystrophy skeletal muscle. *Neurogenetics* **2003**, *4*, 163–171. [[CrossRef](#)] [[PubMed](#)]
43. Screen, M.; Jonson, P.H.; Raheem, O.; Palmio, J.; Laaksonen, R.; Lehtimaki, T.; Sirito, M.; Krahe, R.; Hackman, P.; Udd, B. Abnormal splicing of NEDD4 in myotonic dystrophy type 2: Possible link to statin adverse reactions. *Am. J. Pathol.* **2014**, *184*, 2322–2332. [[CrossRef](#)] [[PubMed](#)]
44. Dadgar, S.; Wang, Z.; Johnston, H.; Kesari, A.; Nagaraju, K.; Chen, Y.W.; Hill, D.A.; Partridge, T.A.; Giri, M.; Freishtat, R.J.; et al. Asynchronous remodeling is a driver of failed regeneration in Duchenne muscular dystrophy. *J. Cell Biol.* **2014**, *207*, 139–158. [[CrossRef](#)]
45. Bakay, M.; Wang, Z.; Melcon, G.; Schiltz, L.; Xuan, J.; Zhao, P.; Sartorelli, V.; Seo, J.; Pegoraro, E.; Angelini, C.; et al. Nuclear envelope dystrophies show a transcriptional fingerprint suggesting disruption of Rb-MyoD pathways in muscle regeneration. *Brain J. Neurol.* **2006**, *129*, 996–1013. [[CrossRef](#)]
46. Vulih-Shultzman, I.; Pinhasov, A.; Mandel, S.; Grigoriadis, N.; Touloumi, O.; Pittel, Z.; Gozes, I. Activity-dependent neuroprotective protein snippet NAP reduces tau hyperphosphorylation and enhances learning in a novel transgenic mouse model. *J. Pharmacol. Exp. Ther.* **2007**, *323*, 438–449. [[CrossRef](#)] [[PubMed](#)]
47. Mollinedo, P.; Kapitansky, O.; Gonzalez-Lamuno, D.; Zaslavsky, A.; Real, P.; Gozes, I.; Gandarillas, A.; Fernandez-Luna, J.L. Cellular and animal models of skin alterations in the autism-related ADNP syndrome. *Sci. Rep.* **2019**, *9*, 736. [[CrossRef](#)]
48. Maimon, R.; Ionescu, A.; Bonnie, A.; Sweetat, S.; Wald-Altman, S.; Inbar, S.; Gradus, T.; Trotti, D.; Weil, M.; Behar, O.; et al. miR126-5p Downregulation Facilitates Axon Degeneration and NMJ Disruption via a Non-Cell-Autonomous Mechanism in ALS. *J. Neurosci. Off. J. Soc. Neurosci.* **2018**, *38*, 5478–5494. [[CrossRef](#)]
49. Gozes, I.; Barnstable, C.J. Monoclonal antibodies that recognize discrete forms of tubulin. *Proc. Natl. Acad. Sci. USA* **1982**, *79*, 2579–2583. [[CrossRef](#)]

50. Alcalay, R.N.; Giladi, E.; Pick, C.G.; Gozes, I. Intranasal administration of NAP, a neuroprotective peptide, decreases anxiety-like behavior in aging mice in the elevated plus maze. *Neurosci. Lett.* **2004**, *361*, 128–131. [[CrossRef](#)]
51. Sragovich, S.; Malishkevich, A.; Piontkewitz, Y.; Giladi, E.; Touloumi, O.; Lagoudaki, R.; Grigoriadis, N.; Gozes, I. The autism/neuroprotection-linked ADNP/NAP regulate the excitatory glutamatergic synapse. *Transl. Psychiatry* **2019**, *9*, 2. [[CrossRef](#)]
52. Dangoor, D.; Biondi, B.; Gobbo, M.; Vachutinski, Y.; Fridkin, M.; Gozes, I.; Rocchi, R. Novel glycosylated VIP analogs: Synthesis, biological activity, and metabolic stability. *J. Pept. Sci. Off. Publ. Eur. Pept. Soc.* **2008**, *14*, 321–328. [[CrossRef](#)]
53. Schmittgen, T.D.; Livak, K.J. Analyzing real-time PCR data by the comparative C(T) method. *Nat. Protoc.* **2008**, *3*, 1101–1108. [[CrossRef](#)] [[PubMed](#)]
54. CRISPOR. Available online: <http://crispor.tefor.net/> (accessed on 15 August 2018).
55. Ran, F.A.; Hsu, P.D.; Wright, J.; Agarwala, V.; Scott, D.A.; Zhang, F. Genome engineering using the CRISPR-Cas9 system. *Nat. Protoc.* **2013**, *8*, 2281–2308. [[CrossRef](#)]
56. Weintraub, A.S.; Li, C.H.; Zamudio, A.V.; Sigova, A.A.; Hannett, N.M.; Day, D.S.; Abraham, B.J.; Cohen, M.A.; Nabet, B.; Buckley, D.L.; et al. YY1 Is a Structural Regulator of Enhancer-Promoter Loops. *Cell* **2017**, *171*, 1573–1588.e28. [[CrossRef](#)] [[PubMed](#)]
57. Kutner, R.H.; Zhang, X.Y.; Reiser, J. Production, concentration and titration of pseudotyped HIV-1-based lentiviral vectors. *Nat. Protoc.* **2009**, *4*, 495–505. [[CrossRef](#)] [[PubMed](#)]
58. Kutner, R.H.; Puthli, S.; Marino, M.P.; Reiser, J. Simplified production and concentration of HIV-1-based lentiviral vectors using HYPERFlask vessels and anion exchange membrane chromatography. *BMC Biotechnol.* **2009**, *9*, 10. [[CrossRef](#)] [[PubMed](#)]
59. Kyriakou, E.I.; van der Kieft, J.G.; de Heer, R.C.; Spink, A.; Nguyen, H.P.; Homberg, J.R.; van der Harst, J.E. Automated quantitative analysis to assess motor function in different rat models of impaired coordination and ataxia. *J. Neurosci. Methods* **2016**, *268*, 171–181. [[CrossRef](#)] [[PubMed](#)]
60. Liang, Y.; Zhang, J.; Walczak, P.; Bulte, J.W.M. Quantification of motor neuron loss and muscular atrophy in ricin-induced focal nerve injury. *J. Neurosci. Methods* **2018**, *308*, 142–150. [[CrossRef](#)] [[PubMed](#)]
61. Marques-Aleixo, I.; Santos-Alves, E.; Mariani, D.; Rizo-Roca, D.; Padrao, A.I.; Rocha-Rodrigues, S.; Viscor, G.; Torrella, J.R.; Ferreira, R.; Oliveira, P.J.; et al. Physical exercise prior and during treatment reduces sub-chronic doxorubicin-induced mitochondrial toxicity and oxidative stress. *Mitochondrion* **2015**, *20*, 22–33. [[CrossRef](#)]
62. al-Hachim, G.M.; al-Khatim, A.S. Prenatal effects of aqueous plastic extract on offspring. *Fetal Diagn.* **1997**, *12*, 28–31. [[CrossRef](#)]
63. Vincent, A.E.; Rosa, H.S.; Alston, C.L.; Grady, J.P.; Rygiel, K.A.; Rocha, M.C.; Barresi, R.; Taylor, R.W.; Turnbull, D.M. Dysferlin mutations and mitochondrial dysfunction. *Neuromuscul. Disord. NMD* **2016**, *26*, 782–788. [[CrossRef](#)] [[PubMed](#)]
64. Bailey, E.C.; Alrowaished, S.S.; Kilroy, E.A.; Crooks, E.S.; Drinkert, D.M.; Karunasiri, C.M.; Belanger, J.J.; Khalil, A.; Kelley, J.B.; Henry, C.A. NAD⁺ improves neuromuscular development in a zebrafish model of FKRP-associated dystroglycanopathy. *Skelet. Muscle* **2019**, *9*, 21. [[CrossRef](#)] [[PubMed](#)]
65. Schaum, N.; Lehallier, B.; Hahn, O.; Palovics, R.; Hosseinzadeh, S.; Lee, S.E.; Sit, R.; Lee, D.P.; Losada, P.M.; Zardeneta, M.E.; et al. Ageing hallmarks exhibit organ-specific temporal signatures. *Nature* **2020**, *583*, 596–602. [[CrossRef](#)] [[PubMed](#)]
66. Tabula Muris, C. A single-cell transcriptomic atlas characterizes ageing tissues in the mouse. *Nature* **2020**, *583*, 590–595. [[CrossRef](#)]
67. String. Available online: <https://string-db.org/> (accessed on 15 July 2020).
68. Goodier, J.L.; Soares, A.O.; Pereira, G.C.; DeVine, L.R.; Sanchez, L.; Cole, R.N.; Garcia-Perez, J.L. C9orf72-associated SMCR8 protein binds in the ubiquitin pathway and with proteins linked with neurological disease. *Acta Neuropathol. Commun.* **2020**, *8*, 110. [[CrossRef](#)]
69. Wei, C.; Stock, L.; Schneider-Gold, C.; Sommer, C.; Timchenko, N.A.; Timchenko, L. Reduction of Cellular Nucleic Acid Binding Protein Encoded by a Myotonic Dystrophy Type 2 Gene Causes Muscle Atrophy. *Mol. Cell. Biol.* **2018**, *38*. [[CrossRef](#)]
70. Gao, Z.; Herrera-Carrillo, E.; Berkhout, B. Delineation of the Exact Transcription Termination Signal for Type 3 Polymerase III. *Mol. Therapy. Nucleic Acids* **2018**, *10*, 36–44. [[CrossRef](#)]

71. Sragovich, S.; Merenlender-Wagner, A.; Gozes, I. ADNP Plays a Key Role in Autophagy: From Autism to Schizophrenia and Alzheimer's Disease. *Bioessays News Rev. Mol. Cell. Dev. Biol.* **2017**, *39*. [[CrossRef](#)]
72. Lukas, Z.; Falk, M.; Feit, J.; Soucek, O.; Falkova, I.; Stefancikova, L.; Janousova, E.; Fajkusova, L.; Zaoralkova, J.; Hrabalkova, R. Sequestration of MBNL1 in tissues of patients with myotonic dystrophy type 2. *Neuromuscul. Disord. NMD* **2012**, *22*, 604–616. [[CrossRef](#)]
73. Byers, T.J.; Beggs, A.H.; McNally, E.M.; Kunkel, L.M. Novel actin crosslinker superfamily member identified by a two step degenerate PCR procedure. *FEBS Lett.* **1995**, *368*, 500–504. [[CrossRef](#)]
74. Miao, Z.; Ali, A.; Hu, L.; Zhao, F.; Yin, C.; Chen, C.; Yang, T.; Qian, A. Microtubule actin cross-linking factor 1, a novel potential target in cancer. *Cancer Sci.* **2017**, *108*, 1953–1958. [[CrossRef](#)]
75. Lane, T.R.; Fuchs, E.; Slep, K.C. Structure of the ACF7 EF-Hand-GAR Module and Delineation of Microtubule Binding Determinants. *Structure* **2017**, *25*, 1130–1138.e6. [[CrossRef](#)] [[PubMed](#)]
76. Aboonq, M.S.; Vasiliou, S.A.; Haddley, K.; Quinn, J.P.; Bubb, V.J. Activity-dependent neuroprotective protein modulates its own gene expression. *J. Mol. Neurosci. MN* **2012**, *46*, 33–39. [[CrossRef](#)] [[PubMed](#)]
77. Jouroukhin, Y.; Ostritsky, R.; Assaf, Y.; Pelled, G.; Giladi, E.; Gozes, I. NAP (davunetide) modifies disease progression in a mouse model of severe neurodegeneration: Protection against impairments in axonal transport. *Neurobiol. Dis.* **2013**, *56*, 79–94. [[CrossRef](#)] [[PubMed](#)]
78. Kodama, A.; Karakesisoglou, I.; Wong, E.; Vaezi, A.; Fuchs, E. ACF7: An essential integrator of microtubule dynamics. *Cell* **2003**, *115*, 343–354. [[CrossRef](#)]
79. Konno, T.; Ross, O.A.; Teive, H.A.G.; Slawek, J.; Dickson, D.W.; Wszolek, Z.K. DCTN1-related neurodegeneration: Perry syndrome and beyond. *Parkinsonism Relat. Disord.* **2017**, *41*, 14–24. [[CrossRef](#)]
80. Grigg, I.; Ivashko-Pachima, Y.; Hait, T.A.; Korenkova, V.; Touloumi, O.; Lagoudaki, R.; Van Dijck, A.; Marusic, Z.; Anicic, M.; Vukovic, J.; et al. Tauopathy in the young autistic brain: Novel biomarker and therapeutic target. *Transl. Psychiatry* **2020**, *10*, 228. [[CrossRef](#)]
81. CTCFBSDB 2.0: A database for CTCF binding sites and genome organization. Available online: <http://insulatordb.uthsc.edu/> (accessed on 15 July 2020).
82. Geiger, R.C.; Taylor, W.; Glucksberg, M.R.; Dean, D.A. Cyclic stretch-induced reorganization of the cytoskeleton and its role in enhanced gene transfer. *Gene Ther.* **2006**, *13*, 725–731. [[CrossRef](#)]
83. Polanco, M.J.; Parodi, S.; Piol, D.; Stack, C.; Chivet, M.; Contestabile, A.; Miranda, H.C.; Lievens, P.M.; Espinoza, S.; Jochum, T.; et al. Adenylyl cyclase activating polypeptide reduces phosphorylation and toxicity of the polyglutamine-expanded androgen receptor in spinobulbar muscular atrophy. *Sci. Transl. Med.* **2016**, *8*, 370ra181. [[CrossRef](#)]
84. Gozes, I.; Iram, T.; Maryanovsky, E.; Arviv, C.; Rozenberg, L.; Schirer, Y.; Giladi, E.; Furman-Assaf, S. Novel tubulin and tau neuroprotective fragments sharing structural similarities with the drug candidate NAP (Davunetide). *J. Alzheimers Dis.* **2014**, *40* (Suppl. 1), S23–S36. [[CrossRef](#)]
85. Malishkevich, A.; Marshall, G.A.; Schultz, A.P.; Sperling, R.A.; Aharon-Peretz, J.; Gozes, I. Blood-Borne Activity-Dependent Neuroprotective Protein (ADNP) is Correlated with Premorbid Intelligence, Clinical Stage, and Alzheimer's Disease Biomarkers. *J. Alzheimers Dis.* **2016**, *50*, 249–260. [[CrossRef](#)] [[PubMed](#)]
86. Kunkel, L.M. To dystrophin and beyond: An interview with Louis Kunkel. *Dis. Models Mech.* **2019**, *13*. [[CrossRef](#)] [[PubMed](#)]
87. Arnett, A.B.; Beighley, J.S.; Kurtz-Nelson, E.C.; Hoekzema, K.; Wang, T.; Bernier, R.A.; Eichler, E.E. Developmental Predictors of Cognitive and Adaptive Outcomes in Genetic Subtypes of Autism Spectrum Disorder. *Autism Res.* **2020**. [[CrossRef](#)]
88. Dresner, E.; Agam, G.; Gozes, I. Activity-dependent neuroprotective protein (ADNP) expression level is correlated with the expression of the sister protein ADNP2: Deregulation in schizophrenia. *Eur. Neuropsychopharmacol. J. Eur. Coll. Neuropsychopharmacol.* **2011**, *21*, 355–361. [[CrossRef](#)]
89. Caballero-Garrido, E.; Pena-Philippides, J.C.; Galochkina, Z.; Erhardt, E.; Roitbak, T. Characterization of long-term gait deficits in mouse dMCAO, using the CatWalk system. *Behav. Brain Res.* **2017**, *331*, 282–296. [[CrossRef](#)] [[PubMed](#)]
90. Simoes, G.F.; Benitez, S.U.; Oliveira, A.L. Granulocyte colony-stimulating factor (G-CSF) positive effects on muscle fiber degeneration and gait recovery after nerve lesion in MDX mice. *Brain Behav.* **2014**, *4*, 738–753. [[CrossRef](#)]
91. Hamers, F.P.; Koopmans, G.C.; Joosten, E.A. CatWalk-assisted gait analysis in the assessment of spinal cord injury. *J. Neurotrauma* **2006**, *23*, 537–548. [[CrossRef](#)]

92. Deumens, R.; Jaken, R.J.; Marcus, M.A.; Joosten, E.A. The CatWalk gait analysis in assessment of both dynamic and static gait changes after adult rat sciatic nerve resection. *J. Neurosci. Methods* **2007**, *164*, 120–130. [[CrossRef](#)]
93. Wooley, C.M.; Sher, R.B.; Kale, A.; Frankel, W.N.; Cox, G.A.; Seburn, K.L. Gait analysis detects early changes in transgenic SOD1(G93A) mice. *Muscle Nerve* **2005**, *32*, 43–50. [[CrossRef](#)]
94. Amende, I.; Kale, A.; McCue, S.; Glazier, S.; Morgan, J.P.; Hampton, T.G. Gait dynamics in mouse models of Parkinson's disease and Huntington's disease. *J. Neuroeng. Rehabil.* **2005**, *2*, 20. [[CrossRef](#)]
95. Carter, R.J.; Lione, L.A.; Humby, T.; Mangiarini, L.; Mahal, A.; Bates, G.P.; Dunnett, S.B.; Morton, A.J. Characterization of progressive motor deficits in mice transgenic for the human Huntington's disease mutation. *J. Neurosci. Off. J. Soc. Neurosci.* **1999**, *19*, 3248–3257. [[CrossRef](#)]
96. Domanskyi, A.; Geissler, C.; Vinnikov, I.A.; Alter, H.; Schober, A.; Vogt, M.A.; Gass, P.; Parlato, R.; Schutz, G. Pten ablation in adult dopaminergic neurons is neuroprotective in Parkinson's disease models. *FASEB J.* **2011**, *25*, 2898–2910. [[CrossRef](#)] [[PubMed](#)]
97. Glajch, K.E.; Fleming, S.M.; Surmeier, D.J.; Osten, P. Sensorimotor assessment of the unilateral 6-hydroxydopamine mouse model of Parkinson's disease. *Behav. Brain Res.* **2012**, *230*, 309–316. [[CrossRef](#)] [[PubMed](#)]
98. Benchaouir, R.; Meregalli, M.; Farini, A.; D'Antona, G.; Belicchi, M.; Goyenvallé, A.; Battistelli, M.; Bresolin, N.; Bottinelli, R.; Garcia, L.; et al. Restoration of human dystrophin following transplantation of exon-skipping-engineered DMD patient stem cells into dystrophic mice. *Cell Stem Cell* **2007**, *1*, 646–657. [[CrossRef](#)]
99. Puzzo, D.; Raiteri, R.; Castaldo, C.; Capasso, R.; Pagano, E.; Tedesco, M.; Gulisano, W.; Drozd, L.; Lippiello, P.; Palmeri, A.; et al. CL316,243, a beta3-adrenergic receptor agonist, induces muscle hypertrophy and increased strength. *Sci. Rep.* **2016**, *5*, 37504. [[CrossRef](#)]
100. Waning, D.L.; Mohammad, K.S.; Reiken, S.; Xie, W.; Andersson, D.C.; John, S.; Chiechi, A.; Wright, L.E.; Umanskaya, A.; Niewolna, M.; et al. Excess TGF-beta mediates muscle weakness associated with bone metastases in mice. *Nat. Med.* **2015**, *21*, 1262–1271. [[CrossRef](#)]
101. Yue, F.; Bi, P.; Wang, C.; Li, J.; Liu, X.; Kuang, S. Conditional Loss of Pten in Myogenic Progenitors Leads to Postnatal Skeletal Muscle Hypertrophy but Age-Dependent Exhaustion of Satellite Cells. *Cell Rep.* **2016**, *17*, 2340–2353. [[CrossRef](#)]
102. Gadalla, K.K.; Ross, P.D.; Riddell, J.S.; Bailey, M.E.; Cobb, S.R. Gait analysis in a Mecp2 knockout mouse model of Rett syndrome reveals early-onset and progressive motor deficits. *PLoS ONE* **2014**, *9*, e112889. [[CrossRef](#)] [[PubMed](#)]
103. Furman, S.; Hill, J.M.; Vulih, I.; Zaltzman, R.; Hauser, J.M.; Breneman, D.E.; Gozes, I. Sexual dimorphism of activity-dependent neuroprotective protein in the mouse arcuate nucleus. *Neurosci. Lett.* **2005**, *373*, 73–78. [[CrossRef](#)]
104. Kapitansky, O.; Giladi, E.; Jaljuli, I.; Bereswill, S.; Heimesaat, M.M.; Gozes, I. Microbiota changes associated with ADNP deficiencies: Rapid indicators for NAP (CP201) treatment of the ADNP syndrome and beyond. *J. Neural Transm.* **2020**, *127*, 251–263. [[CrossRef](#)]
105. Meyfour, A.; Ansari, H.; Pahlavan, S.; Mirshahvaladi, S.; Rezaei-Tavirani, M.; Gourabi, H.; Baharvand, H.; Salekdeh, G.H. Y Chromosome Missing Protein, TBL1Y, May Play an Important Role in Cardiac Differentiation. *J. Proteome Res.* **2017**, *16*, 4391–4402. [[CrossRef](#)] [[PubMed](#)]
106. Boxer, A.L.; Lang, A.E.; Grossman, M.; Knopman, D.S.; Miller, B.L.; Schneider, L.S.; Doody, R.S.; Lees, A.; Golbe, L.I.; Williams, D.R.; et al. Davunetide in patients with progressive supranuclear palsy: A randomised, double-blind, placebo-controlled phase 2/3 trial. *Lancet Neurol.* **2014**, *13*, 676–685. [[CrossRef](#)]

Publisher's Note: MDPI stays neutral with regard to jurisdictional claims in published maps and institutional affiliations.



© 2020 by the authors. Licensee MDPI, Basel, Switzerland. This article is an open access article distributed under the terms and conditions of the Creative Commons Attribution (CC BY) license (<http://creativecommons.org/licenses/by/4.0/>).